

3838

SMALL-ANGLE X-RAY SCATTERING

Helmut Pessen and Thomas F. Kumosinski
United States Department of Agriculture
Eastern Marketing and Nutrition Research Division
Agricultural Research Service
Philadelphia, Pennsylvania 19118

and

Serge N. Timasheff
Pioneering Research Laboratory of Physical Biochemistry
United States Department of Agriculture
Eastern Marketing and Nutrition Research Division
Agricultural Research Service

and

Graduate Department of Biochemistry
Brandeis University
Waltham, Massachusetts 02154

I. Introduction

Among the methods available for the characterization of globular proteins, small-angle X-ray scattering (SAXS) is particularly powerful. This method is capable of yielding the radius of gyration and, when used on the absolute-intensity scale, the molecular weight, hydrated volume, surface-to-volume ratio and degree of hydration of a particle in solution¹⁻⁶. In order to obtain this information, two auxiliary parameters need to be measured: the concentration and the partial specific volume of the protein.

In addition to the molecular parameters, one may obtain thermodynamic parameters of interacting systems^{4,5}, such as association constants of aggregating subunit systems and the degree of preferential interaction of proteins with components of mixed solvent systems. Furthermore, in the case of highly concentrated solutions (> 100 mg/ml), in which there are strong long-range intermolecular interactions, SAXS can be used to determine the radial distribution function of the interacting (or even partly immobilized) macromolecules in solution^{1,5,7,8}. This, in turn, yields the interaction potentials characteristic of the operative forces⁹. At still higher concentrations, distinct bands may appear, as the system gradually becomes ordered and X-ray scattering passes over into small-angle X-ray diffraction¹⁰. The recent development of absolute intensity apparatus^{6,11,12} (see Sect. III.A) has rendered practical such a characterization of macromolecules, and aggregates of molecules,

including enzymes, in solution.

Fundamentally, the method of X-ray scattering differs little from that of light scattering, the theoretical principles being essentially identical. The differences which exist arise from differences in the wavelengths of the radiations in the two cases. In light scattering, the wavelength is of the order of $4,000 \text{ \AA}$; in SAXS it is $\sim 1.5 \text{ \AA}$. Both techniques are based on concentration fluctuations of the solution under examination. In light scattering an auxiliary parameter required is the refractive index increment of the macromolecular solute. This can be measured directly. In SAXS such a measurement is not possible, since the refractive index is practically indistinguishable from unity. In order to express the concentration fluctuations it becomes necessary, therefore, to calculate a corresponding quantity, which for SAXS is the electron density, i.e., the number of electrons per unit volume. This can be done from the chemical compositions of the solution components.

The electromagnetic theory basic to SAXS is also basic to X-ray diffraction, and the two techniques are founded on the same phenomena. They differ, however, in the nature of the observations. X-ray diffraction results from destructive and constructive interferences in scattered radiation, evidenced by discrete spots or bands which correspond to characteristic repeat distances within an ordered structure, such as a crystal. In SAXS the scattered radiation is diffuse and a generally monotone

function of angle. X-ray diffraction reflections usually correspond to small interatomic distances and thus are found at higher angles; SAXS corresponds principally to molecular dimensions and is concentrated mostly within a cone a few degrees from the incident beam. There is an intermediate region (2-5°) in which the internal order of macromolecules begins to manifest itself. This leads to the appearance of secondary maxima and minima superimposed on the scattering curve, resulting in a wave-like appearance of the angular dependence of scattering at these higher angles. As will be shown (see Sect. II. B) below, the positions of these fluctuations in the scattering curve are very useful in assigning structural models to particular macromolecules.

II. Principles

A. Nature of the Phenomenon

When a beam of electromagnetic radiation strikes an electron, some of the energy is momentarily absorbed and the electron becomes displaced from its unperturbed position due to the force exerted on it by the electric field. As a result, the electron is set into periodic motion with a frequency equal to that of the exciting radiation. Since, according to the Maxwell equations, any accelerating or decelerating charge must radiate an electromagnetic wave in all directions and since the radiation reemitted by the electron has the same frequency as the exciting radiation, the experimental observation gives the impression that the incident radiation is scattered in all directions by the electron,

as depicted schematically in Figure 1a. This observation is the origin of the terms "X-ray scattering" as well as "light scattering". In the quantum view the incident X-ray photons undergo perfectly elastic collisions with the electron, leaving their energy (i.e., their frequency) unchanged. Hence this type of scattering is called "elastic", "unmodified", "coherent" and, because it obeys Bragg's law, "Bragg scattering."^{12a}

While a detailed derivation of the theory of X-ray scattering can be found in various monographs^{1,13}, we will outline here briefly the arguments followed. The action of an electric field of strength E on a polarizable particle quite generally induces in it a dipole moment, p , whose magnitude is

$$p = \alpha E \quad (1)$$

where α is a proportionality constant known as the polarizability and is a measure of the induced distortion of the molecule. For an electromagnetic wave, E , the amplitude of the electric field vector can be expressed by

$$E = E_0 \cos 2\pi(\nu t - x/\lambda) \quad (2)$$

where E_0 is the maximum amplitude, ν is the frequency, λ is the wavelength, t is time and x is the location along the line of propagation. Here, the cosine function represents the phase angle, the determination of which is one of the main problems in structure determination by X-ray diffraction. Combining equations 1 and 2, the amplitude, E_s , of the reemitted electric field, which is proportional to d^2p/dt^2 , results in:

$$E_s = - \frac{4\pi^2 v^2}{c^2 r} p \sin \varphi \quad (3)$$

where c is the velocity of light, r is the distance between the scattering particle and the observer and φ is the angle between the dipole axis and the line joining the point of observation to the dipole, as shown in Figure 1b. The intensity, I , of the radiation is equal to the product of the amplitude and its complex conjugate¹³ (the conjugate of a complex quantity $a + ib$ being defined as $a - ib$), $I = EE^*$, whose magnitude is¹⁴

$$I = |E_s|^2 \quad (4)$$

If we take now a source of unpolarized radiation and resolve the scattered radiation into components parallel and perpendicular to the electric vector of the incident radiation, and sum up the total, having first combined equations 1, 2, 3 and 4, and remembering that $c/v = \lambda$, we obtain the familiar Rayleigh equation, which is fundamental for light scattering (see chapter of this volume).

$$I_{\text{scat}} = |E_s|^2 = \frac{8\pi^4 a^2}{r^2 \lambda^4} I_0 (1 + \cos 2\theta) \quad (5)$$

where I_{scat} is the intensity of the scattered radiation, I_0 is that of the incident radiation and 2θ is the angle between the directions of the incident and scattered rays, as defined in Figure 1b¹⁵.

B. Scattering from an Electron

For radiation whose frequency is high compared to the natural frequency of the dipole (as is the case for X-rays, though not for visible light), the polarizability, α , can be expressed as

$$\alpha = \frac{-e^2}{4\pi^2 \nu^2 m} \quad (6)$$

where e is the charge and m is the mass of the scattering element, the electronic charge and electronic mass in the case of an electron. Combination of equations 5 and 6 results in the Thomson equation, which is the fundamental equation of X-ray scattering:

$$I_{\text{scat},e} = \frac{e^4}{m^2 c^4 r^2} I_0 \left(\frac{1 + \cos^2 2\theta}{2} \right) \quad (7)$$

where $I_{\text{scat},e}$ is the scattered intensity from a single, independent electron. The product $e^4 m^{-2} c^{-4}$ is known as the electron scattering factor (also termed electron scattering cross section and Thomson's constant; equal to the square of the so-called electron radius), while the quantity in parentheses is known as the polarization factor¹⁶. Introducing the numerical values of e , m and c , into Equation 7 results in

$$\frac{I_{\text{scat},e}}{I_0} = 7.90 \times 10^{-26} r^{-2} \left(\frac{1 + \cos^2 2\theta}{2} \right) \quad (8)$$

This indicates that the intensity of radiation scattered by a single electron is more than 25 orders of magnitude smaller than

the intensity of the incident beam. Now, the mass of a proton is 1,840 times greater than that of an electron. Since mass appears to the second power in the denominator of Equation 7, scattering by a proton will be ca 3.4×10^6 times weaker than that by an electron. As a result, in X-ray scattering, as well as in X-ray diffraction, essentially only the electrons in matter are detected. This has given rise to the term "electron density"¹⁷ and to the practice in X-ray scattering of expressing all mass units in numbers of electrons.

While the scattering from a single electron is extremely weak, in real systems, such as a protein in aqueous medium, we measure the total scattering from all the electrons in the irradiated volume (which is of the order of 0.1 ml). This results in a measured scattered intensity only 10^4 to 10^5 times weaker than the incident radiation. Such an intensity is measurable, but the four to five orders of magnitude difference in intensities between the incident and scattered radiations lead to the extremely stringent instrument collimation requirements which will be discussed below (See Sect. III.A).

C. Scattering from Particles

1. Scattering Envelope

In molecules, such as those of proteins, the electrons are not independent, since the relative positions of the atoms are fixed in space. It is reasonable, therefore, to expect interactions between the scattering of individual electrons. Since the dimensions of macromolecules are always large relative to the wavelength of the incident X-radiation, interference occurs between

the radiation scattered from individual scattering elements (in the case of X-ray scattering, these are individual electrons) within the macromolecule, with the result that the intensity of scatter is a strong function of the angle of observation, 2θ . The reason for this is shown in Figure 2a. Here we have a particle which is large with respect to the wavelength of the radiation. Consider scattering from elements n and m observed at points P and Q . We find that when radiation scattered by elements n and m reaches point P (in the forward direction), if angle 2θ is small, the difference between the pathlengths of the two rays ($nP + mP - nP$) is small, so that they are not greatly out of phase with each other and interference is small. However, when the radiation scattered from n and m reaches point Q (in the backward direction) the total distance traveled by the ray from m is much greater than that from n (greater by $nQ + mQ - nQ$), with the result that the two rays can become completely out of phase, leading to destructive interference. In the forward direction, i.e., along the incident beam, scattered radiation from n and m is fully in phase, there is no interference and the total scattering is the sum of the scatterings from all elements within the particle. As a result, the scattering envelope (i.e., the angular dependent of the scattering) has an asymmetric shape such as shown schematically in Figure 2b. (For clarity, the envelope is shown much less elongated than should actually be the case.) Since scattering in the forward direction falls on top of the much stronger incident beam it cannot be measured directly. This results in the requirement of extrapolation to zero angle. The

shape of a typical recording of the angular dependence of scattering of X-rays obtained from a protein solution is shown in Figure 2c. At very low angles, the angular dependence of the scattering is essentially gaussian. At increasing values of 2θ (above 1°), the intensity drops to very low values, decreasing asymptotically to a constant background value. In this higher angle region, secondary maxima and minima become superimposed on the weak and diminishing radiation.

a. Debye Equation. In 1915 Debye¹⁸ showed that the angular dependence of the scattering from a particle of any shape, averaged over all orientations, is given by

$$I_{\text{scat}}(s) = \sum_{m=1}^N f_m \sum_{n=1}^N f_n \frac{\sin 2\pi s r_{nm}}{2\pi s r_{nm}} \quad (9)$$

$$s = (2/\lambda) \sin \theta$$

where N is the total number of scattering elements in the particle, f_m and f_n are the scattering factors of any pair of scattering element, r_{nm} is the distance between elements n and m , λ is the wavelength of the radiation and 2θ is the angle between the incident and scattered beams. From this equation, the angular dependence of the scattering of variously shaped bodies can be calculated by introducing specific expressions for r_{nm} , characteristic of the geometry of the particular body. The approximate shape of a scattering particle can be determined by comparing the experimental scattering envelope with envelopes calculated for various geometric models. It is not necessary, however, to know the shape of a particle to obtain certain information about its

structure.

b. Guinier Equation; Radius of gyration. In 1939 Guinier¹⁹ showed that scattering yields a characteristic geometric parameter of any particle which is independent of any assumption regarding its shape, namely the radius of gyration, R_G , i.e., the root-mean-square of the distances of all the electrons of the particle from its center of electronic mass. Expanding Equation 9, Guinier showed that in the case of isotropic particles for a point source radiation, and for small values of the product $R_G s$,

$$i_n(s) = i_n(0) \left(1 - \frac{4}{3} \pi^2 R_G^2 s^2 + \dots \right) \approx i_n(0) \exp(-4/3 \pi^2 (R_G)^2 s^2) \quad (10)$$

where $i_n(s)$ is the scattered intensity at angle 2θ corresponding to a given value of s , (normalized to the energy of the incident beam, i.e., referred to the scattering produced by a single electron under the identical conditions; See Sects. III.A and IV.A); $i_n(0)$ is the normalized intensity extrapolated to zero angle. Thus, at very low angles, a plot of $\log i_n(s)$ versus s^2 gives a straight line (Figure 3a), the slope of which is $(4/3) \pi^2 R_G^2$. As will be shown below, the intercept, $i_n(0)$, is proportional to the square of the molecular weight.²⁰

As a practical matter, it is rarely possible to utilize a point source, on account of its insufficient intensity. The geometry generally chosen for the source is one defined by a narrow slit (See Sect. III.A). If the slit is long, so that its height

exceeds the angular range, measured at the detector, at which observable scattering occurs, it is said to be an "infinitely high" slit. In analogy to Equation 10, the normalized scattering intensity $j_n(s)$ from an infinite-slit source is given by^{1,3}

$$j_n(s) = j_n(0) \exp(-4/3\pi^2 R_a^2 s^2) + \phi(s) \quad (11)$$

where $j_n(0)$ is $j_n(s)$ extrapolated to zero angle, R_a is the apparent radius of gyration, i.e., that referring to a finite concentration of solute, and $\phi(s)$ is a residual function expressing the difference between the gaussian portion of Equation 11 and the scattering actually observed.

c. Deconvolution. The theoretical point-source scattering curve can be constructed from the experimental infinite-slit data by an appropriate mathematical transformation¹ which is fairly simple in principle but, in practice, is attended with considerable difficulties. It is usually carried out numerically on a digital computer. Using the Luzzati³ form of this transformation, $i_n(s)$ and $j_n(s)$ are related by

$$i_n(s) = -\frac{1}{\pi} \int_0^\infty \frac{dj_n(s^2+t^2)^{1/2}}{d(s^2+t^2)^{1/2}} \frac{dt}{(s^2+t^2)^{1/2}} \quad (12)$$

2. Molecular Weight

If in Equation 9 each scattering element is taken as one electron in the particle, and the particle contains m electrons,

then it can be shown that, for a single particle in vacuum, $i_n(0) = m^2$. For J non-interacting particles, the total scattering at $2\theta = 0^\circ$ is Jm^2 . Expressing the concentration in mass per volume units, c , $J = c/m$, in vacuum,

$$\frac{i_n(0)}{c} = m \quad (13)$$

Now, passing to the real case of macromolecules in solution, the fluctuation theory of scattering^{21,22} gives for a two component system, e.g. an enzyme dissolved in water, the following relation between the excess scattering of solution over solvent, $\Delta i_n(0) = i_n(0)_{\text{solution}} - i_n(0)_{\text{solvent}}$, and the fluctuations of the electron density, $\overline{\Delta \rho_s^2}$, in a volume element of volume δV :

$$\Delta i_n(0) = V \delta V \overline{\Delta \rho_s^2} \quad (14)$$

Here, V is the total irradiated volume and ρ_s is the electron density of the solution (number of electrons per unit volume).

Since

$$\overline{\Delta \rho_s^2} = \left(\frac{\partial \rho_s}{\partial c_e} \right)_{T, p} \overline{\Delta c_e^2} \quad (15)$$

where c_e is the solute concentration expressed as the ratio of

the number of electrons of solute to that of solvent (essentially a molal concentration), application of the thermodynamic relations for concentration fluctuations²² results in

$$\left(\frac{\partial \rho_s}{\partial c_e}\right)_{T,p}^2 \frac{c_e}{\Delta i_n(o) \rho_1^2} = \frac{1}{m_{app}} = \frac{1}{m} \left[1 + \frac{c_e}{RT} \left(\frac{\partial \mu_e}{\partial c_e}\right)_{T,p} \right] \quad (16)$$

where ρ_1 is the electron density of the solvent, R is the gas constant, T is the thermodynamic temperature, μ is the chemical potential of the solute and m_{app} is an apparent mass (in electrons) of the particle calculated for each finite concentration of protein at which scattering measurements are made.²³ Since the electron density increment, $\left(\frac{\partial \rho_s}{\partial c_e}\right)_{T,p}$ is not a directly

measurable quantity, it must be replaced in a working equation by one which is readily measurable. At constant temperature and pressure,

$$\frac{d\rho_s}{dc_e} = \rho_1 (1 - \rho_s \psi_2) \quad (17)$$

where ψ_2 is the electron partial specific volume of the solute. In studies on enzymes, the measurements are performed in solution; thus the intensity value used is the excess scattering of solution over solvent, $\Delta i_n(s)$. For the sake of simplicity, we will drop the symbol Δ , taking note that in what follows, $i_n(s)$ and $j_n(s)$ refer to the excess scattering. Combining Equations 13 through 17,

expressing the derivative of the excess chemical potential, μ^e , of solute with respect to concentration as the usual virial expansion, such as used in light scattering and osmometry,²² and setting $\rho_s \approx \rho_l$ (since at low solute concentrations, the electron densities of solvent and solution will be the same within experimental error), leads to

$$m_{\text{app}} = i_n(0) (1 - \rho_l \psi_2)^{-2} c_e^{-1} \quad (18a)$$

and

$$m = m_{\text{app}} + 2Bm^2 c_e \quad (18b)$$

where B is the second virial coefficient. Extrapolation to zero concentration of a plot of $1/m_{\text{app}}$ vs. c_e leads, then, to m from the ordinate intercept and, with m known, to B from the slope. The molecular weight, M, is readily obtained from m, since

$$M = mN_A/q, \quad (19)$$

where q is the number of electrons per gram of the particle, calculated from its chemical composition, and N_A is Avogadro's number.

3. Other Parameters

For an isotropic particle of uniform electron density, at large values of s, and using slit optics,^{1,24}

$$\lim_{s \rightarrow \infty} s^3 j_n(s) = \lim_{s \rightarrow \infty} s^3 j_n^*(s) + \delta^* s^3$$

(20)

$$j_n^*(s) \equiv j_n(s) - \delta^*$$

where $\lim_{s \rightarrow \infty} s^3 j_n(s) \equiv A$ and δ^* are constants and $j_n^*(s)$ is a

corrected normalized scattering intensity defined by the equation. A plot of $s^3 j_n(s)$ vs. s^3 follows the form shown in Figure 3b: as s^3 increases, the product $s^3 j_n(s)$ first increases rapidly in non-linear fashion; at sufficiently high values of s^3 this function assumes a linear form, with weak fluctuations superimposed on it. The intercept of the straight line portion of this plot is A and its slope is δ^* . As has been shown by Luzzati et al²⁴, δ^* reflects the internal structure of the macromolecule. Knowledge of A and $j_n^*(s)$ permits the calculation of several other molecular parameters²⁴.

The external surface area, S , of the particle in solution, is given by^{3,25,26}

$$S = 16\pi^2 A (\rho_2 - \rho_1)^{-2} \quad (21)$$

where ρ_2 is the mean electron density of the hydrated particle. The hydrated volume, V , can be obtained by integration under the scattering curve,

$$V = \frac{i_n(0)}{\int_0^\infty 2\pi s j_n^*(s) ds} = \frac{m(1 - \rho_1 \psi_2)^2 c_e}{\int_0^\infty 2\pi s j_n^*(s) ds} \quad (22)$$

It may be shown that the surface-to-volume ratio is

$$\frac{S}{V} = \frac{8\pi A}{\int_0^\infty s j_n^*(s) ds} \quad (23)$$

The excess electron density of the hydrated particle over that of solvent, $\Delta\rho = \rho_2 - \rho_1$, can be calculated from

$$\Delta\rho = \frac{\int_0^{\infty} 2\pi s j_n^*(s) ds}{c_e (1 - \rho_1 \psi_2)} + \rho_2 c_e (1 - \rho_1 \psi_2) \quad (24)$$

The degree of hydration, H , expressed as the ratio of the number of electrons of water of hydration to the number of electrons of the dry particle, is

$$H = \frac{\rho_1 (1 - \rho_2 \psi_2)}{\Delta\rho} \quad (25)$$

The exact values of the parameters of equations 22-25 are obtained by extrapolation to zero protein concentration.

With a knowledge of a number of molecular parameters--namely, M , R_G , V and S/V -- the possible overall geometry of the unknown particle becomes highly restricted. Further information on the particle shape may be obtained from scattering at higher angles. At these angles ($2\theta > 2^\circ$), the X-ray scattering curves develop maxima and minima superimposed on the Guinier relationship. The positions of these are well defined for different geometric models, and scattering curves for various models have been calculated (See Sect. IV.E). Comparison of the experimental curves with those calculated for various likely models then suggests the choice most compatible with the data.

4. Multicomponent Systems

All of the foregoing relations are rigorously valid only

for true two-component systems, such as a macromolecular solute immersed in pure solvent, e.g. an enzyme in water. In biological systems we normally deal with thermodynamically more complicated multicomponent systems, the additional components being buffer salts, dispersing agents, or other perturbants. The proper interpretation of data requires, therefore, the application of multicomponent thermodynamic theory. In practice, it is found that in dilute buffers (≤ 0.2 M) the multicomponent effects are negligibly small and in most cases the above two-component equations may be used directly. In the case of some enzymes, however, the solution properties of the macromolecules are such that a dispersing agent must be added at high concentration (e.g. concentrated salt, urea or organic solvents). In such a case, just as in light scattering and equilibrium sedimentation, the parameters measured contain a contribution from the interactions between the macromolecule and solvent components. Multicomponent fluctuation theory yields for small-angle X-ray scattering an equation for the molecular weight similar to that obtained in light scattering (See chapter of this volume). Defining^{27,28} principal solvent as component 1, enzyme as component 2, and the additive as component 3, we have^{5,29}

$$\frac{c_{e,2} \left(\frac{\partial \rho}{\partial c_{e,2}} \right)_{T,p,c_{e,3}}^2}{i_n(0) \rho_0^2} = \frac{1}{m_2(1+D)^2} \left[1 + \frac{c_{e,2}}{RT} B' \right]$$

$$D = \frac{\left(\frac{\partial \rho}{\partial c_{e,3}} \right)_{T,p,c_{e,2}}}{\left(\frac{\partial \rho}{\partial c_{e,2}} \right)_{T,p,c_{e,3}}} \left(\frac{\partial c_{e,3}}{\partial c_{e,2}} \right)_{T,p,\mu_3} = \quad (26)$$

$$= \frac{(1-\rho_1\psi_3)}{(1-\rho_1\psi_2)} \left(\frac{\partial c_{e,3}}{\partial c_{e,2}} \right)_{T,p,\mu_3}$$

where the symbols have their previous meaning, and B' is a complicated function of interactions between the various components, identical to that found in light scattering (See chapter of this volume). In order to obtain the true molecular weight in such a system, it becomes necessary to measure the extent of preferential interaction, i.e., $(\partial c_{e,3} / \partial c_{e,2})_{T,p,\mu_3}$ between the enzyme and solvent components in an auxiliary experiment, for example by equilibrium dialysis. The various geometric parameters also become complex, since solvent interactions result in the fluctuating unit being no longer isotropic; as a result, the values obtained from equations 11, 21, 22, and 23 can serve only as qualitative estimates. Equations taking multicomponent effects into account can be developed, however, for the shape parameters.

5. Polydispersity

If the particles present vary in molecular weight and size, the observed scattering is the sum of contributions from all components. The Guinier equation then becomes

$$\frac{i_n(s)}{Kc_e} = \frac{\sum i_n(s)_i}{K \sum c_{e,i}} = \frac{\sum c_{e,i} m_i}{\sum c_{e,i}} \left(1 - \frac{4}{3} \pi^2 s^2 \frac{\sum c_{e,i} m_i R_{G,i}^2}{\sum c_{e,i} m_i} \right) \quad (27)$$

The values of the molecular weight and radius of gyration obtained in such systems are, then, the weight average molecular weight and a radius of gyration of an average which is a function of the particle shape³⁰.

D. General Remarks

1. Resolution

Similarly to other methods which measure the size and shape of macromolecules, the resolution of small-angle X-ray scattering can be defined as the limit of molecular dimensions that can readily be measured. In discussing this question, it is expedient to compare small-angle X-ray scattering to the related technique of light scattering. Resolution can be expressed essentially in terms of the highest value of the radius of gyration that can be measured. Since the validity of the Guinier equation (eq. 10) is an approximation based on the assumption that $R_G^2 s^2 \ll 1$, in practical terms this reduces the question to that of the lowest value of the angular parameter, s (see equation 9), attainable. In light scattering, with radiation of $\sim 4,000 \text{ \AA}$ wavelength, and the usual limits of angular measurements being ca. $2\theta = 20^\circ$, the limit of attainable s^{-1} is $\sim 1.2 \times 10^4 \text{ \AA}$. The Guinier equation then imposes an upper value of $\sim 1,200 \text{ \AA}$ for the radius of gyration experimentally accessible. Similarly, in small-angle X-ray scattering, the wavelength is 1.5 \AA , while the smallest angle that can be readily reached is ca. $10'$; thus, the limit of attainable s^{-1} is $\sim 540 \text{ \AA}$. This sets 55 \AA as an upper limit for the radius of gyration that can be reasonably measured. For a spherical protein, $R_G^2 = \frac{3}{5} r^2$ (where r is the radius of the sphere); this sets 65 \AA as the maximal value for the measurable radius which corresponds to a molecular weight of ca. 300,000. The converse of this relation is the limit of the lowest molecular

dimensions that can be detected. In light scattering this is of the order of $\lambda/10$, or ca. 400 \AA ; in small-angle X-ray scattering, since the wavelength is very small, there is, in principle, no similar limit. In practice, however, the low intensities of scattering from biological macromolecules require a minimal molecular dimension of $\sim 10 \text{ \AA}$.

When the overall dimensions of a particle are large compared to the maximal resolution attainable, i.e., when $R_G^2 s^2$ is not small, the angular dependence of scattering no longer obeys the Guinier equation. Relations can be developed, however, for the angular dependence of the scattered intensity for particular structural models. For example, in the case of long asymmetric structures, such as those encountered in myosin, collagen, or in the associated form of glutamate dehydrogenase,³¹ the parameters which are readily obtainable are the cross-section radius of gyration, R_c , i.e., the radius of gyration for rotation about the long axis, and the mass per unit length, m/l , of the equivalent rigid rod. The corresponding scattering equation is:³²

$$j_n(s) = \frac{m}{2l} c_e (1 - \rho_1 \psi_2^2) \exp(-\pi^2 R_c^2 s^2) K_0(\pi^2 R_c^2 s^2) \quad (28)$$

"el"

where m is mass in electrons, l is length in \AA and the other symbols have their previous meaning; K_0 indicates a kappa function.

A striking example of the differences in resolution between light scattering and small-angle X-ray scattering is shown in

Fig. 4, where a comparison is given of the structural features observed by the two techniques for DNA and ribosomal RNA. In small-angle X-ray scattering, DNA appears as a rigid rod with cross-sectional dimensions characteristic of a Watson-Crick double helix.³² In light scattering, where ten times greater dimensions are viewed, DNA appears as a stiff worm-like chain.^{33,34} The heavy (32 S, 1.9×10^6 molecular weight) component of ascites tumor cell ribosomal RNA is seen in light scattering as an asymmetric globular structure with a radius of gyration of 355 Å,^{4,35} while small-angle X-ray scattering at ten times greater resolution shows that this molecule is actually a zig-zag chain composed of double-helical segments ca. 85 Å in length linked by flexible joints.^{4,36,37} It should be pointed out, furthermore, that if the small-angle X-ray scattering experiments on the RNA had been limited to angles greater than 1° (i.e., $s^{-1} < 85 \text{ \AA}$), the angular dependence of scattering would have been that characteristic of a rigid double-helical rod. This example shows how two related techniques which view molecular dimensions at different resolutions can be used to great advantage together to obtain rather detailed structural information on macromolecules in solution and to compare the geometric features of two structurally related molecules

2. Limitations

The method of small-angle X-ray scattering is almost unique in its ability to give simultaneously geometric and thermodynamic parameters of macromolecules in solution; it also has great

limitations and is best used late in a study, i.e. on already well defined systems. The principal limitation stems from the low intensity of scattering and the necessity to perform measurements at angles very close to the incident beam. This imposes the instrumental requirement of an extremely fine degree of collimation, which will be discussed below (see Sect. III.A). The second difficulty, related to the low intensities, is the necessity to use slit sources of radiation. The theoretical equations describing the angular dependence of the scattering from structures of various shapes, however, have been derived for a point source. This requires the use of mathematical transformations such as equation 12 to "desmear" the data (see below, Sect. IV.B); such operations are not feasible without the use of computers. Related also to the low intensity of scattering are two additional limitations. One is the need to use lengthy scans (~24 hours per concentration point) in order to record a sufficient number of counts over the angular range normally covered (from $+8^\circ$ to -8° , see below, Sect. III.B). The other is the necessity to use high protein concentrations (5-70 mg/ml). Therefore, in a highly nonideal system, such as an enzyme at a pH far from its isoionic point, the product $2Bmc_e$ of equation 18, could become very large, introducing great uncertainty into the measured molecular weight. In an associating system, the data would fall essentially into the concentration range where the aggregated species predominate. In such systems it is best to combine the application of small-angle X-ray scattering with that

of other thermodynamic techniques, such as light scattering and sedimentation equilibrium, in which the measurements are performed over progressively decreasing concentration ranges. Such a comparison is shown in Figure 5 for the association of β -lactoglobulin A. As can be seen, good agreement can be obtained between sedimentation equilibrium³⁸, which gives the details of the reaction in the low concentration range, light scattering, which is used to characterize the middle and high concentration ranges^{39,40} and small-angle X-ray scattering⁴¹.

The fact that the small-angle X-ray scattering data are available at high concentrations has, however, the advantage that, in an associating system, the radius of gyration measured is essentially that of the enzyme polymer. This follows directly from the types of averages which are measured. Just as in light scattering, small-angle X-ray scattering yields the weight-average molecular weight and a higher-order average radius of gyration,

$$\overline{R_G^2} = \frac{\sum_i c_i M_i R_{G,i}^2}{\sum_i c_i M_i} \quad (29)$$

Since the relation of the radius of gyration to the molecular weight is a function of the shape of the particle, this average can be complicated. The proper relations for a variety of geometric models have been tabulated elsewhere^{29,30}.

3. The Role of Dust

The higher-order average of the radius of gyration measured in small-angle X-ray scattering, together with the form of the

Guinier equation, an exponential in $-s^2 R_G^2$, leads to an experimental simplification. Namely, the "dust problem", familiar in light scattering (See chapter)^{42,43} is not found in small-angle X-ray scattering. "Dust" particles are so large that their scattering is almost fully in the forward direction. Thus, when angles of $> 5'$ are reached, i.e. the angular range in which small-angle X-ray scattering measurements usually begin, there is no significant contribution remaining from "dust" scattering. As a result, as a practical matter, small-angle X-ray scattering does not require the elaborate solution clarification techniques normally used in light scattering.

III. Experimental

A. Apparatus

I. Basic Requirements

Despite the similarity, or even basic identity, of small-angle X-ray scattering (SAXS) theory to the theory of light scattering, instrumentation for measuring the corresponding phenomena has taken quite different forms.

In principle, both techniques require the same basic apparatus components: (a) a radiation source, (b) means for selecting desired wavelengths from this source, (c) a collimating system for ensuring a desired geometry for the irradiating beam, (d) a sample holder or, in the case of samples in solution, a sample vessel or cell, (e) some type of goniometer arrangement for allowing observation of the scattered radiation over a range of

precisely defined angles with respect to the incident radiation, (f) a radiation detector mounted on the movable arm of the goniometer, and (g) a data readout with optional ancillary data-processing equipment. (In an earlier stage of development, and occasionally still in use today for certain purposes, the function of the last three components is performed by appropriately arranged photographic film. These are subsequently evaluated with a densitometric device to relate the intensities of the photographic record to angular positions ^{whence} / the apparatus is referred to as a "scattering camera.")

As a practical matter, the special characteristics of X-rays have made it necessary for X-ray scattering apparatus to assume very particular forms. Furthermore, the slow development of the apparatus over the past four decades has reflected the special interests and personal approaches of individual workers in the field, many of whom attempted designs of their own, few of which ever have become commercialized.

In the following, the main features, as well as the most prominent instruments illustrative of a given type will be described briefly. Since scattering is a general phenomenon of which diffraction may be considered to constitute a particular case, it will not be surprising that many of the less specialized apparatus components used for X-ray scattering are the same as those familiarly used in X-ray diffraction equipment. In fact, the term "diffractometer" is frequently used to refer to a SAXS apparatus comprising a goniometer, as contrasted to one comprising

a camera. In view of the variety of relevant design features and, at the same time, the scarcity of models in general use, the principal special requirements, many of which are inter-related, will first be considered in some detail.

2. Special Requirements

a. Stability of Source and Apparatus. Scattering is a quantum process, hence a random event, and acceptable counting statistics presuppose a certain minimum number of counts.⁴⁴ Since dilute solutions of biological macromolecules are weak scatterers (typical scattered intensities at 1° scattering angle might be of the order of 20 to 100 counts/second) the accumulation of the requisite number of counts, whether measured continuously or discretely at a number of points over the angular range of interest, involves relatively long total counting times, of the order of 12 to 24 hours, and sometimes more. During this entire time, the intensity of the primary beam is expected to remain constant, as is every other parameter of the instrument, such as its geometric relationships and the detector gain. These considerations, which are of no concern in the case of a camera, are matters of great consequence with a detector instrument.

Stability of the detector and of the signal-processing electronics may be achieved by the use of stabilized power supplies and by suitable design and selection of electronic components to assure negligible drift. Physical stability to assure maintenance of the relative positions of all the apparatus ele-

ments, such as source, slits, sample, and detector, is achieved by proper mechanical design, including choice of dimensions, materials of construction, balance, methods of support, and fastenings of components. Source and goniometer are usually mounted on a rigid steel or marble plate, often the top of a commercial X-ray generator. (In the construction of our instrument we have made use of the rigidity afforded by an eight-inch thick granite slab.) In addition, dimensional changes due to temperature fluctuations should be controlled by ambient air conditioning to within $\pm 0.5^{\circ}\text{C}$, with special avoidance of exposure to transient temperature extremes; i.e., the apparatus should not be directly exposed to the stream of air issuing from the conditioning system, and it is desirable to shield it by air locks from less well-controlled air from adjacent rooms. Variations in barometric pressure and humidity, because of their effects on proportional detectors and on static charges which may affect the measuring system, have also been found to be detrimental.^{45,46}

Stability of the X-ray source has presented much more of a problem. It is necessary to start with an X-ray generator incorporating a high degree of voltage regulation and tube-current stabilization. Diffraction tubes generally employ water cooling to protect the life of the targets. Close temperature control (to $\pm 1^{\circ}\text{C}$) of this cooling water, though not usually important in diffraction work, is essential in scattering work to maintain the dimensional stability of the target, as otherwise the focal spot will tend to wander, compromising the delicate alignment of

the scattering apparatus. Instruments employing crystal monochromators (to be discussed below), which image the narrow focal spot of a fine-focus tube (typically, 0.4 x 8.0 mm), are more sensitive to even slight focal-spot wandering (of the order of a fraction of a micrometer) than are pure slit-collimating instruments. In these the slits eliminate a relatively large portion of the much larger focal spot of a regular tube in order to produce the narrow primary beam required and a slightly shifted focal spot will still completely illuminate the slits. Since higher intensity primary beams will yield higher scattered intensities and thus allow shorter counting times or scans, high-power tubes have been employed using currents in excess of 80 ma, as compared with currents nearer 25 ma for a fine-focus tube. However, to dissipate the heat generated by the electrons bombarding the anode at this rate, rotating anodes have to be used. The rotating motion and the slight vibration involved again aggravate the problem of focal spot wander.⁴⁷

Despite all measures taken to obtain stability of the entire system, the primary beam will still be found to have some tendency to drift over the relatively long experimental times involved. Detection of this drift, and possible correction for it, has been attempted by monitoring the beam intensity. Practical difficulties inherent in this approach have prevented it from being adopted to any great extent in scattering work, although a recent design of a monitor system has been described by Kratky et. al.⁴⁸. The application of signal averaging, a technique increasingly used to improve signal-to-noise ratio (e.g., in nuclear magnetic resonance work), has been suggested^{49,50}, though

again not widely adopted.

In the absence of a monitoring device, it is not possible to establish directly whether the primary beam intensity had remained constant throughout an extended experiment. An indirect check on constancy, however, can be obtained by virtue of the near-perfect symmetry of the scattered intensities on the two sides of zero angle which is a characteristic of a well-aligned instrument. This is accomplished by folding a chart record of intensity vs. angle at the zero angle position and examining by means of an illuminator whether the two branches of the recorded curve are coincident. If instability due to any cause, in any part of the total system, has occurred during an experiment, it is virtually certain to manifest itself here as a lack of symmetry, since the likelihood of one kind of disturbance being precisely compensated by another is vanishingly small. It goes without saying that the chart paper may not be opaque, and also that this valuable check is not available unless the scattering instrument is so designed as to allow measurements on both sides of the direct beam.

b. Quality of Source. Beyond the aspects of stability and intensity, mentioned in the preceding section, the cross section of the primary beam, and hence the focal spot, is required to be homogeneous and, for the slit optics discussed below, it must be of rectangular rather than of trapezoidal or other shape. Particularly with crystal monochromatization, the effect of any deviation from these requirements becomes readily noticeable.

The spectral purity of the radiation obtained from the tube is of great importance, especially if the primary beam is not monochromatized. In the absence of other monochromatization, even the use of a pulse-height analyzer does not yield sufficiently fine energy resolution to prevent smearing of the scattering curve due to the energy distribution.⁵¹

Even an uncontaminated target and tube producing pure copper radiation, the radiation most often chosen for SAXS, does not yield radiation of a single wavelength since, depending on the relation of the exciting potential to the Duane-Hunt short-wavelength limit,⁵² varying amounts of the copper continuum and of characteristic radiation other than the desired K_{α} line are present. A pulse-height analyzer can eliminate the continuum and the unwanted characteristic lines, including nearly all of the K_{β} , though not the higher harmonics of the K_{α} line if the potential is high enough to excite them. The use of balanced filters, i.e., a combination of Ni and Co filters of the proper thickness whose absorption edges bracket the Cu K_{α} line, will accomplish the same result, but in either case the K_{α} line will still consist of the K_{α_1} - K_{α_2} doublet. A well aligned high quality crystal monochromator, on the other hand, can separate this doublet and yield the K_{α_1} , the larger component, free from all but traces amounting to a few percent of the K_{α_2} .^{53,54}

Monochromator crystals may be flat, but they yield higher intensities when bent. In the configuration of "Johann"⁵⁵, a thin crystal plate, elastically or plastically bent to a radius of

curvature R (Figure 6), focuses rays from the source S , diffracted by an angle θ obeying Bragg's law, approximately to point F , where S , F , and the center of the crystal face lie on a circle (the Rowland circle) having a diameter equal to the radius of curvature of the bent crystal. This crystal is tangent to the circle, since the radius of the circle is only one-half the radius of curvature of the crystal. For exact focusing, the face of the crystal must be ground to be coincident with, rather than just tangent to, the circle according to Johansson.^{56,57} This latter technique is more exacting, the crystals are much more costly, and the anticipated increase in intensity due to more perfect focusing is frequently not realized because of other deviations from ideality, so that the Johann type crystals are the ones more generally used. For $\text{Cu } K_{\alpha}$ radiation, quartz laminae, elastically bent, have been found most suitable. The 1011 lattice planes are the ones utilized; by cutting the crystal faces at an angle α (typically, 8°) to these planes, a desirable asymmetry results which allows a more favorable geometry for the instrument. With this method, the intensity of the focal spot is better utilized, and a longer optical path is made available for the slit system, because the monochromator may be located much closer to the source, than would be possible with a symmetrically cut crystal.⁵⁸ Since for a given spacing d and angle θ , Bragg's law, $n\lambda = 2d \sin \theta$, is satisfied by only ^{one} value of $n\lambda$, true monochromatization (except for the admission of harmonics) is achieved.

c. Slit Geometry. Scattering theory has been derived for a point source. Point sources or, more realistically, spot sources are so weak in intensity that they have been employed in few instruments. Customarily, one resorts to a source having a negligible extension in only one dimension, i.e., an illuminated slit, which produces a beam of narrow rectangular cross section. Such a slit or line source can be conceived of as consisting of a large number of spot or point sources along a straight line, and the scattering curves produced by such a slit are derived from those produced by a point source by the "smearing", or superposition, of a large number of the latter, in a manner corresponding to the mathematical operation of convolution. In order to be evaluated, such so-called "slit-smeared" experimental curves generally must be "de-smeared" or deconvoluted. In practice, this is not always a simple matter. Numerous methods, graphical, analytical, and numerical, have been described.⁵⁹⁻⁶⁶

For this deconvolution, the actual intensity distribution of the longitudinal beam profile must be known. The mathematics become somewhat simpler if the assumption of an infinite slit height may be made, i.e., if the height of the slit is greater than the arc length over which the detector can see any appreciable scattering.

The earliest slit geometry still in common use employs four slits (see Sect. III.A), the first close to the source, the second close to, and just ahead of the sample, and two more slits between sample and detector. The first two are collimating slits

whose function is to remove all but a thin, nearly parallel bundle of rays from the primary beam coming from the source. The third is the receiving slit; it defines the angular position at which the detector reads the intensity. The fourth is an anti-scatter slit, which prevents the detector from seeing any scattered or parasitic radiation from directions other than the irradiated volume of the sample.

Use of a curved-crystal monochromator leads to a second slit geometry (see Sect. III.A). The monochromator described in the preceding section, besides selecting the desired wavelength, also performs a focusing function. Whereas the four-slit geometry selects from the widely diverging beam issuing from the X-ray tube window a very thin and only very slightly diverging beam, the monochromator focuses a widely diverging beam, and thus concentrates a converging beam on the sample and the detector. There is little, if any, net gain in intensity, since various losses due to the monochromator are large enough to outweigh the collimation losses due to the first two slits of the pure four-slit system. The monochromator still requires the use of four slits; however, the first two slits in this system no longer have a collimating function. The purpose of the first slit is solely to eliminate parasitic radiation produced by scattering from the monochromator holder and elsewhere, while the second slit removes radiation scattered from the edges of the first. The quality of these two slits and their adjustment (and particularly that of the second slit) are exceedingly critical in

this system, as is the fine adjustment of the monochromator itself to the exact focusing position. The number of elements which must be in precise alignment makes this system very dependent on effective provisions to facilitate these potentially very time-consuming adjustments.

A third geometry, that of Kratky (see Sect. III.A), is particularly successful in eliminating parasitic radiation originating from slit edges and, thus, is capable of very high resolution. In place of the initial two slits it uses a precisely machined asymmetric system of steel blocks to produce a region virtually free of parasitic scattering very close to one side of the direct beam, albeit at the price of making inaccessible to observation one half of the scattering region, namely that on the other side of the direct beam.

Still other, less generally used collimating systems will be described together with the specific instruments which use them (See Sect. III.A).

d. Resolution and Angular Range. The problems of the geometric definition of the beam and of the elimination of parasitic scatter-

c. Slit Geometry. Scattering theory has been derived for a point source. Point sources or, more realistically, spot sources are so weak in intensity that they have been employed in few instruments. Customarily, one resorts to a source having a negligible extension in only one dimension, i.e., an illuminated slit, which produces a beam of narrow rectangular cross section. Such a slit or line source can be conceived of as consisting of a large number of spot or point sources along a straight line, and the scattering curves produced by such a slit are derived from those produced by a point source by the "smearing", or superposition, of a large number of the latter, in a manner corresponding to the mathematical operation of convolution. In order to be evaluated, such so-called "slit-smeared" experimental curves generally must be "de-smeared" or deconvoluted. In practice, this is not always a simple matter. Numerous methods, graphical, analytical, and numerical, have been described.⁵⁹⁻⁶⁶

For this deconvolution, the actual intensity distribution of the longitudinal beam profile must be known. The mathematics become somewhat simpler if the assumption of an infinite slit height may be made, i.e., if the height of the slit is greater than the arc length over which the detector can see any appreciable scattering.

The earliest slit geometry still in common use employs four slits (see Sect. III.A), the first close to the source, the second close to, and just ahead of the sample, and two more slits between sample and detector. The first two are collimating slits

whose function is to remove all but a thin, nearly parallel bundle of rays from the primary beam coming from the source. The third is the receiving slit; it defines the angular position at which the detector reads the intensity. The fourth is an anti-scatter slit, which prevents the detector from seeing any scattered or parasitic radiation from directions other than the irradiated volume of the sample.

Use of a curved-crystal monochromator leads to a second slit geometry (see Sect. III.A). The monochromator described in the preceding section, besides selecting the desired wavelength, also performs a focusing function. Whereas the four-slit geometry selects from the widely diverging beam issuing from the X-ray tube window a very thin and only very slightly diverging beam, the monochromator focuses a widely diverging beam, and thus concentrates a converging beam on the sample and the detector. There is little, if any, net gain in intensity, since various losses due to the monochromator are large enough to outweigh the collimation losses due to the first two slits of the pure four-slit system. The monochromator still requires the use of four slits; however, the first two slits in this system no longer have a collimating function. The purpose of the first slit is solely to eliminate parasitic radiation produced by scattering from the monochromator holder and elsewhere, while the second slit removes radiation scattered from the edges of the first. The quality of these two slits and their adjustment (and particularly that of the second slit) are exceedingly critical in

this system, as is the fine adjustment of the monochromator itself to the exact focusing position. The number of elements which must be in precise alignment makes this system very dependent on effective provisions to facilitate these potentially very time-consuming adjustments.

A third geometry, that of Kratky (see Sect. III.A), is particularly successful in eliminating parasitic radiation originating from slit edges and, thus, is capable of very high resolution. In place of the initial two slits it uses a precisely machined asymmetric system of steel blocks to produce a region virtually free of parasitic scattering very close to one side of the direct beam, albeit at the price of making inaccessible to observation one half of the scattering region, namely that on the other side of the direct beam.

Still other, less generally used collimating systems will be described together with the specific instruments which use them (See Sect. III.A).

d. Resolution and Angular Range. The problems of the geometric definition of the beam and of the elimination of parasitic scattering are central to the design of any SAXS instrument. Aside from the geometry of the goniometer, the precision of its position readout and any associated gearing, and the width of the receiving slit, the resolution of the instrument depends on the width of the primary beam at the receiving slit. In all the systems mentioned, narrowness of the primary beam is achieved to a great extent at the expense of its intensity, so that a compromise has to be reached between the precision with which data may be obtained and

the concentration at which the sample may be studied, or its inverse, the extended time required for the study, with its attendant drawbacks. Nevertheless, the monochromator system, because of its converging beam, and the Kratky system, because of its freedom from parasitic scattering, have inherent advantages over the four-slit system with its diverging beam and substantial parasitic scattering from its collimating slits.

Some of the information of interest in SAXS is contained in the data at the smallest angles and, because of the inverse relationship between d and θ indicated by the Bragg law, the larger the molecules (or particles) studied, the smaller these angles. Yet, the smallest angles (forward scattering, close to zero angle) are experimentally inaccessible because they are occupied by the primary beam which, owing to its finite width, must extend some distance on either side of the zero angle. Being of the order of $10^5 - 10^6$ times more intense than the adjacent scattered intensities produced by all but the strongest scatterers, it will mask these as soon as they overlap. It is true that, to protect the detector, the primary beam is invariably blocked in X-ray work by a heavy-metal beam stop or some equivalent device, but this provision itself leads to some degradation of data. If the beam stop, or its equivalent, is slightly too wide, it will block also the measurement of some otherwise detectable scattered radiation; if it is slightly too narrow, it will allow some of the direct beam to spill over and swamp scattered radiation. Furthermore, the primary beam is not truly a sharp beam entirely confined to a limited angular region.

The so-called rocking curve, the curve of beam intensity vs. angle, has tails extending out to fairly large angles (except in the case of some double-crystal instruments, where these tails may be very sharply limited). The tails are exceedingly faint compared to the peak intensity, but they are by no means negligible on the millionfold smaller scale of the scattered radiation.

It is clear then that the collimation or narrowness of the beam, besides influencing the general precision of the data, determines the small-angle limit. It can be readily appreciated that the aforementioned requirements are particularly sensitive to the problems of stability, discussed ^{above} (See Sect. III.A). In fact, it may be said that the greatest single difficulty in designing a SAXS instrument resides in this complex of requirements.

Other information of value is obtained from scattering at relatively high angles, up to about 8° . Here the scattered intensities are very low. To obtain measurements within reasonable counting times it is desirable to work with as much scattering material as possible, i.e., with relatively high concentrations. There are, however, practical upper limits to the usable concentrations of protein solutions, and thus the counting times are inevitably lengthened. Again, the requirement for long-term stability makes itself felt here.

e. Absolute-Scale Intensity Measurements. Absolute-scale measurements allow the calculation of particle parameters not readily obtained otherwise, as discussed in the section on prin-

ciples (See Sect. II.C). Absolute-scale intensity or, for short, absolute intensity, or absolute-unit measurements, may be defined fundamentally as the intensity scattered by the sample at any angle in terms of the intensity scattered by a single classical electron under the same conditions, i.e., expressed in electron units⁶⁷. For working purposes it has been defined in terms of the ratio of the scattered intensity to that of the incident beam.^{68,69} These two definitions, and yet others, may not be entirely equivalent, the second one being not necessarily independent of the collimation system; a more detailed discussion may be found elsewhere.⁷⁰

The chief experimental difficulty consists in measuring the intensity of the primary beam. The intensity of the unattenuated primary beam, as mentioned above, is so much greater than the scattered intensity that the two cannot be directly measured on the same scale by any practical apparatus. In fact, the unattenuated direct beam is much too intense for the counting speed of even modern X-ray detecting devices with few exceptions.⁷¹ Hence, for any direct comparison with the scattered radiation, it must be attenuated or sampled in some precisely defined manner.

Attenuation by calibrated filter foils^{11,68,72,73,74} by utilization of the Bragg reflection from a perfect Si crystal⁷⁵, or by fractional-time sampling of the beam by means of a rotating disk with a calibrated hole^{69,76} have all been employed with some success, although each method has its own difficulties. The filter method requires flaw-free foils of very uniform thickness, and the calibration of a set of filters to the required accuracy is a

very time-consuming procedure, again depending on stable radiation. The anomalous transmission method and the rotating-disk method are, unlike the foil method, experimentally awkward and not well adapted to routine use. Indeed, the rotating-disk method has been used essentially in only one laboratory, where it has served in the calibration of a large number of secondary standards, which in turn are employed, there and elsewhere, in measurements where scattered intensities are in this way indirectly referenced to their respective primary beams⁴⁵.

Indirect comparison with the primary beam can be accomplished by reference to a standard scatterer which may be a primary or a secondary standard. Use of a secondary standard, a sample calibrated by means of one of the direct methods just mentioned has been the method chosen by Kratky and collaborators, employing samples of polyethylene.⁷⁷⁻⁷⁹ It is an absolute requirement that the standard possess long-term physical, chemical, and radiation stability; the last problem, in particular, appears not to have been completely solved.

The second indirect method of comparison is by establishing a primary standard by calculation of its scattering properties from basic data.⁷² This approach is feasible for gases,^{80,81,82} gold sols^{83,84} and silica gels.⁸⁵ The number of materials suitable for such standards is limited and the measurement of their intensities is apt to take very long. Thus, this method also is not suitable for routine use. In addition, the further the physical state of the standard differs from that of the samples to be studied (protein solutions, in our case), the more will the

geometry of the setup be inevitably different, and comparability of the two types of measurements becomes questionable.

f. Alignment Provisions and Other Apparatus Features. In designing SAXS apparatus, overriding consideration must be given to adequate provisions for adjusting the many elements (monochromator, slits, sample holder, scanning arm pivot and detector) through which the incident and the scattered beams are required to pass. Each has a number of degrees of freedom and the proper alignment of several of these is quite critical. Moreover, these alignment provisions must also assure stability.

Regarding precision and repeatability, these provisions may range in various instruments from simple manual shifting of entire apparatus subassemblies on their supports, and their maintenance in position simply by gravity, to motions in dovetailed or ball-bearing tracks, controlled by precision or differential screws. Position indications, if provided, may be by simple scales, with or without vernier, by dial indicator or, most often, by micrometer heads. Part of the reason for the popularity of micrometer heads is the fact that they combine the positioning and indicating functions in one relatively compact device. Where fairly large adjustment forces as well as great positional accuracy is required, a separate drive in conjunction with a dial indicator may be more suitable.

If the scattering apparatus is intended for one type of application only, flexibility and general accessibility of the apparatus are not essential factors. If studies are to extend

to a variety of materials, temperatures, concentrations, states of aggregation, or particle sizes, an apparatus permitting various adjustments and the use of possible accessories becomes desirable. Almost inevitably, there must be some sacrifice of stability, because an adjustable element, unless especially well constructed, is never quite as rigid as a similar fixed one, and an accessible apparatus layout will tend to be more spacious and not as rigid as a more compact one. Good mechanical design, however, can minimize any detrimental consequences of such a compromise.

One factor in this respect is the spatial orientation of the apparatus. The great majority of designs have utilized a horizontal layout, i.e., one in which the scanning motion is in a horizontal plane (confusingly, this is sometimes referred to as "vertical," because the motion is about a vertical axis). Some major designs (those of Kratky and Skala⁸⁶ and of Luzzati et. al.¹¹) use a vertical motion (and, consequently, a horizontal axis), as do some successful standard X-ray diffractometers (e.g., that manufactured by Philips⁸⁷).^{87a} The advantage of the vertical design follow from its inherent compactness: savings in floor space, and possibly (but not necessarily) increased rigidity. In diffraction work it is customary to use an X-ray generator whose top surface fulfills the function of a work table, with the X-ray tube mounted, tower fashion, on its center. If the tube is thus mounted vertically, a four-window tube housing allows the use of as many as four instruments (diffractometers,

cameras, or other accessories) at the same time. This results in a highly efficient utilization not only of the available space but also of the operating capacity and of the limited life of the tube.⁸⁸

Because of the generally increased compactness, with the apparatus, so to speak, extending into the air, flexibility and general accessibility are somewhat diminished compared to a horizontal layout. If, in order to permit an extended angular range of observation, the goniometer is mounted on a vertical base plate, the various subassemblies must be mounted and various adjustments must be performed in this generally cramped vertical plane, in which even temporarily placed components need to be clamped to remain in place. Similar steps are simpler and more convenient on a horizontal table. A horizontal instrument can be modified much more readily, with fewer problems of maintaining mechanical balance and original rigidity. It must be understood that a horizontal instrument, having vertical slit requirements, requires a horizontally mounted tube, either or both of whose vertical line-source windows will be thus available. One of the spot-source windows will be pointing downward and will be unusable, and the other will be pointing upward and will not be conveniently usable. This is hardly a sacrifice, since the spot sources are rarely utilized in an apparatus primarily devoted to scattering work.

3. Survey of Existing Instruments

a. Slit-Collimation Instruments. Early designs of slit instruments incorporated three slits, two collimating slits and one

guard slit ahead of the sample. The choice of the various dimensions for optimum results has been discussed extensively^{89,90,91} and a number of cameras have been built on this basis (e.g. Hoseman).⁹²

By way of digression, it may be noted here that camera-type instruments almost invariably have provisions for a vacuum path, for two reasons. The first, which applies to goniometer instruments as well, is the reduction of absorption losses by air, which increase the intensity problem. The second reason lies in the parasitic scattering produced in the air volume between sample and detector. As pointed out by Luzzati¹¹, this scattering is serious in the case of a camera because the entire emulsion is subject to it during the whole period of exposure, but is less serious in the case of a goniometer. Here the presence of a third and a fourth slit between sample and detector limits the direction from which parasitic scattering can impinge on the detector at any one time to the very small amount arising along the line of the scattering angle at that time, since a goniometer involves a sequential method of detection. As a result, vacuum chambers are frequently not used with goniometers, and if used, they are usually found only between the sample and the detector.

The addition of another slit results in the four-slit geometry, Fig. 7, favored by Beeman⁹³ and his collaborators^{81,94} and still currently used. In order to obtain sufficient intensity, rotating X-ray anodes are frequently used with this type of instrument. Absolute intensity work, when undertaken, has utilized

comparison with scattering from a standard gas (See Sect. III.A). A commercial form of this type of apparatus (but without special provisions for absolute measurements, and without symmetrically adjustable slits) is the instrument manufactured by Rigaku Denki, Ltd., Tokyo, distributed in the U.S. by Engis, Inc. Instruments of this kind have been used in the study of biological solutions by Anderegg et al.⁹⁴, Ritland et al.⁹⁵, and Brierre⁹⁶.

b. Crystal Monochromator Instruments. A goniometer instrument with a monochromator consisting of a flat crystal has been described by Kahovec and Ruck⁹⁷. Most designs, however, have taken advantage of the observations of Guinier⁵⁸ that (a) curved crystals yield both greater intensity and the advantages of focusing, and (b) asymmetrically cut curved crystals, following a suggestion by Fankuchen⁹⁸, have considerable practical advantages (See Sect. III.A). The resulting geometry (Fig. 8) shows the angle of convergence of the primary beam, ω , and the region b, subject to parasitic scattering, which limits the definition of the primary beam. The relative advantages of this system have been discussed by Guinier and Fournet⁹⁹, as have those of various more complicated systems using double crystal monochromatization. Because of increased complexity, the latter, while having certain uses for X-ray diffraction, are not practical for routine SAXS work.

A method of using a Guinier-type instrument, without vacuum chamber, in such a manner as to cancel various constants

peculiar to the instrument and its geometry has been devised by Luzzati and co-workers^{11,68}. Whereas all instruments mentioned so far have been horizontal, that of Luzzati, which makes use of the commercial Philips goniometer, is vertical. It uses a fine-focus tube in conjunction with a curved-quartz monochromator, calibrated nickel-foil filters for absolute measurements, and a Geiger-Müller tube or proportional counter for detection. A further development of this type of instrument has been described by Pessen et al.^{6,100}, Fig. 9. It uses the same method for absolute measurements as that of Luzzati, but differs from it by the use of a horizontal goniometer, a sealed-window proportional detector in conjunction with a pulse-height analyzer, and various instrument refinements. These two instruments have found extensive use in studies of biological materials in solution. An attempt along similar lines has been made by Renouprez et al.¹⁰¹ whose instrument has been used in the study of solid catalysts. Another diffractometer utilizing crystal monochromatization and aiming at high resolution, ease in alignment and rigidity of construction is that of Kavesh and Schultz¹⁰², who used it in studies of crystalline polymers. No SAXS diffractometers of these various types are commercially available, although the components for the Luzzati instrument are available from commercial sources.

c. Block-Collimation Instrument. A highly original solution to the parasitic scattering problem which limits ultimate resolution is embodied in the Kratky instrument¹⁴³. As the diagrams (Fig. 10) of the collimating system show, parasitic scattering

from slit edges is suppressed to an extraordinary degree by means of a special arrangement of blocks with highly finished surfaces, which replace a more conventional slit system. As mentioned above (See Sect. III.A), it is an unavoidable consequence of this system that one-half of the primary beam is blanked out before it reaches the sample, and only one side of a scattering curve is observable. For absolute measurements, secondary standards (polyethylene samples standardized against an intensity-attenuating rotating disk) are routinely employed (See Sect. III.A.2.e., above). Like the Luzzati instrument, this one has a vertical goniometer. It should be noted that, unlike the Luzzati-type instruments described in the preceding section which are constructed to satisfy the assumptions of the "infinite slit," the Kratky instrument, depending on the construction of the X-ray tube used with it, may require^{that} a weighting function descriptive of the primary-beam longitudinal profile be used in the deconvolution calculations. This instrument is particularly well constructed with respect to compactness and rigidity. Manufactured by Anton Paar, KG (Graz, Austria), and distributed

by the Siemens Group and by Sefert and Co. (Ahrensburg, W. Germany) around the world, it is at present the SAXS instrument in widest use. It has been employed extensively in studies of biological solutions^{31,103-105}.

d. Other and Special Instruments. The problem of slit-smearing can be avoided by use of a point focus. Simple pinhole collimation to obtain a point focus, however, results in unacceptably

severe intensity losses. These losses can be somewhat alleviated by using focusing crystals. A single, spherically bent quartz crystal has been used in a scattering instrument constructed by Hagström and Siegbahn¹⁰⁶. Henke and DuMond¹⁰⁷ have constructed an instrument in which a monochromatic point-focus beam is produced by total reflection from an ellipsoidal mirror. Combinations of two crossed cylindrically bent crystals have also been used. Shenfil et al.¹⁰⁸ used two quartz crystals in reflection; Furnas¹⁰⁹ used a mica crystal in transmission, crossed with a quartz crystal in reflection. Franks¹¹⁰ used total reflection from two crossed bent glass plates. The Franks camera has been built commercially and distributed in the U.S. by the Jarrell-Ash Co.

Such instruments may be adapted to meet the requirements of high resolution, as well as irradiation of a very limited area of the specimen of interest, for instance, where a fine-grained poly-crystalline material is to be examined. Still, their intensity is generally too low to allow the study of weakly scattering solutions of biological materials.

A variation on the ellipsoidal mirror consists in the more efficient toroidal mirror of Elliott¹¹¹. Cameras allowing the optional use of double Franks' mirror optics or Elliott toroid optics, developed by G.D. Searle, Ltd., are available from Elliot Automation Radar Systems, Ltd. in England, represented by Picker Corporation in the U.S.. They have been applied to studies

of polymers, tissues and cell constituents, and to biological macromolecules in the solid form, such as nucleic acids, conjugated proteins, and polypeptides.

Among other special designs is a high-resolution camera built by Brumberger and Deslattes¹¹², which utilizes the Borrmann effect, in which a germanium crystal of fairly high perfection is used in anomalous transmission to give an astigmatic image of the source. Another effect utilized for monochromatization is that of multiple total reflections from opposite sides of a groove in a single silicon crystal, described by Bonse and Hart¹¹³, Fig. 11. As a consequence of the repeated reflections there occurs a progressive enhancement of the peak-to-background ratio of the reflection curve. A second grooved crystal, located between sample and detector, is rotated to perform the scanning. The result is probably the sharpest peak available from any instrument, having negligible tails, and suitable for extremely high-resolution work. An instrument designed by Koffman¹¹⁴ which uses this principle is manufactured by AMR and distributed in the U.S. by Philips Electronic Instruments. Its performance compared to that of the Kratky instrument has been evaluated by Kratky and Leopold¹¹⁵. It appears that, although producing more intensity than point-focus instruments, the repeated reflections / result in such losses that the intensity left is insufficient for the study of weak scatterers, such as proteins in solution.

B. Procedure

1. Introduction

SAXS is a versatile method that has been applied to the study of a wide variety of systems in different fields, among which are particle and pore sizes in catalysts, grain sizes and clustering in alloys, ceramics and glasses, critical phenomena, colloidal micelles, crystallinity in polymers, order in tissue constituents, and biopolymers in solution. It is to be expected that each application dictates practical aspects peculiar to its requirements. Here we are concerned only with the study of macromolecules (predominantly globular proteins) in solution. In what follows, we will confine ourselves mainly to the procedures which are currently being used in our laboratory and which are further developments of the methods of Luzzati. While some of the methods may not be strictly applicable to a different apparatus setup, this material should be illustrative of the general approach taken in this type of work.

The experimental procedure may be divided into preliminary steps, namely those performed only once (such as filter calibration), or only once for a series of runs (such as apparatus alignment, if called for by a test for alignment), and operational steps, which have to be performed individually for each sample run. These may be either preparatory (preparation of sample, determination of protein concentration, determination of partial specific volume and measurement of cell thickness), or they may be the actual data gathering, i.e., measurements

of primary beam intensities and of scattered intensities as a function of scattering angle. They will be discussed in this order.

2. Preliminary Steps.

a. Filter Calibration. As indicated above, measurements of incident-beam intensity require that a set of calibrated attenuating filters be at hand. The basic construction requirement is freedom from pinholes. In addition to careful selection of the nickel foils used, the chances of inhomogeneities being present are further reduced by building up each filter to the requisite thickness from layers of thinner foils, so that very slight imperfections will tend to average out. The most efficient design of a set of filters is one in which the filter factors are so related that each of the denser filters is approximately equivalent to exactly one combination of the less dense ones. (One or two of the lower values may be constructed in duplicate, to facilitate arranging various combinations.) Thus, a series of factors such as 2^1 , 2^2 , 2^4 , 2^8 , ... is suitable. A further requirement is that the densest filter be adequate to get the count rate at the peak of the primary beam down to a value which is not only measurable with the equipment available, but which is also below the range where the counting-system dead-time correction and the peak shift of the pulse-height distribution become of importance. Practical count rates of less than 20,000 counts/second at a peak rate of perhaps 10 million counts/second (without filter) require a filter

factor of over 500.

With a filter of that approximate value (although initially it is not known precisely) in place, the attenuation factors of each of the less dense filters in the series may be determined by measuring in turn the intensity of a stable beam without, and with, the unknown less dense filter in place, and taking the ratio of the respective intensities. When a sufficient number of the less dense filters have been calibrated in this manner to approximately equal, in combination, the attenuation factor of the unknown densest filter, the combination of the less dense filters is placed in the filter holder and the beam intensities without, and with the densest filter added are determined in turn. Their ratio gives the filter factor of the latter. Because of the propagation of errors, it is evident that the attainment of a desired precision in the attenuation value of the densest filter requires a very much higher precision of each of the less dense filters. Fortunately, this tends to be the case anyway, since during equal counting intervals a less dense filter will accumulate larger counts, resulting in lower relative counting errors. In each determination, the counting interval must be long enough to accumulate a total count sufficiently large to give a ^{low} relative error, as determined by counting statistics.⁴⁴

During the time of filter calibration constancy of the beam intensity must be ascertained by periodic checks. If a change has been detected by monitoring and can be well defined,

it may be possible to correct for it. Corrections for counting-system dead-time, although much smaller for proportional counters than for Geiger-Müller counters, also must be applied separately for each filter. The subject is discussed in some texts on X-ray diffraction and elsewhere^{11, 75, 116, 117}.

b. Apparatus Alignment. Alignment is a particularly exacting process. It starts with the monochromator. The bending press, which clamps the crystal lamina to give the required curvature, is mounted on a horizontally rotatable platform in such a way that the center of rotation coincides with the center of the concave front face of the elastically deformed crystal. With the X-rays on and the shutter open (suitable shielding precautions having been taken) manipulation of, first, the coarse, and finally, the fine rotational adjustment (the latter by means of a sensitive differential tangent screw) will bring the monochromatized beam corresponding to the K_{α} line into view on a fluorescent screen in the dark. The monochromator platform is supported so as to permit a variety of adjustments, axial, transverse vertical and horizontal, and rotary in a vertical plane. All these adjustments may have to be applied in an iterative fashion until near-perfect alignment is accomplished. The criterion for perfect alignment of a good crystal is the presence of a rectangular and homogeneous beam cross-section and its sudden appearance and disappearance, without shifts in position, upon a slight change of the horizontal rotatory fine adjustment in either direction.¹¹⁸

Next, the goniometer table as a whole is adjusted to align the first two slits with the monochromatized beam. (These slits, which are continuously adjustable and symmetrically opening and closing) must be optically aligned beforehand, so that their median lines and the goniometer axis of rotation lie in the same vertical plane. The goniometer table is mounted on two superimposed platforms, each of which allows a mode of adjustment. The lower platform allows translation transverse to the optical axis of the monochromatized primary beam; this motion is actuated by a differential screw and may be read on a dial indicator. The upper platform is designed to be rotatable about a pivot which can be adjusted to coincide with the median line of the first slit; this rotation is actuated by a two-speed screw, allowing both coarse and fine adjustment, and is similarly dial-indicated. The primary beam, visualized by a fluorescent screen, is first threaded through the first slit by translation of the lower platform. Next, the second slit is opened wide, and the sample holder is replaced with an auxiliary slit mounted and aligned in such a way that its median line coincides with the goniometer axis. The primary beam is then threaded through the auxiliary slit by rotation of the upper platform, the first slit remaining essentially in place.

The detector is now aligned approximately. The first and the auxiliary slits define the zero-angle position and, with the third and fourth slits removed, the goniometer readout is adjusted to zero, using the detector in conjunction with a strip-

chart record. The third and fourth slits are replaced and adjusted so that they just admit the primary beam to the detector. The second slit is replaced last and is adjusted until it just fails to graze the primary beam. Its purpose is to eliminate edge-scattering produced by the first slit; its edges must not be irradiated by the primary beam, leading to further parasitic scattering. The quality of this slit and its alignment are exceedingly critical. The final test is a constant-speed scan from about 0.5° on one side of zero to 0.5° on the other, with the intensity versus time recorded on a strip chart. Until a symmetrical scan is obtained, some, or all, of the preceding adjustments may have to be repeated one or more times. The first two slits are then opened to the desired width, which is defined by the smallest angles to be measured in a given experiment. Since frequently, it is necessary to carry out in sequence runs with different slit openings, it is advantageous to have the slit openings controlled by micrometer heads; it should become, then, a matter of routine to open and close these slits as required.

3. Preparatory Steps.

a. Sample Preparation. Since all molecular parameters must be evaluated by extrapolation to infinite dilution (See Section II), it is necessary in every case to study a concentration series. Hence a series of protein concentrations, obtained by dilution from a stock solution, must be so chosen that the points are as far separated as possible in order to yield well-defined concen-

tration plots for the various parameters. The upper limit to the concentrations may be set by the availability of a scarce material, by its limited solubility, or by excessive viscosity of more concentrated solutions; it rarely exceeds 100 g/l. The lower limit is imposed by the technique itself. In the case of biological macromolecules, even moderately dilute solutions (much under 10 g/l) produce so little excess scattering that, given the random nature of the radiation process, the difference between solution and solvent scattering is not sufficient to yield statistically meaningful results.

The scattering we are concerned with is the excess scattering, i.e. the scattering due to the macromolecular solute of interest alone. As shown in Section I (See also Chapter of this volume), this means that the solvent used for the blank measurements must have a chemical potential identical to that of the solvent as it exists in the solution. Hence, ideally the solvent used as blank for each protein dilution must be the dialyrate of that particular dilution. In practice, when the concentrations of the non-aqueous components of the solvent are low, e.g. 0.1 M salt, this is sufficiently approximated by using the dialyrate of the stock solution as reference solvent and as diluent.

These considerations differ little from those applicable to any other thermodynamic technique, for example light scattering. Fortunately, as pointed out above (See Sect. II.D) the very troublesome problem encountered in light scattering, namely

the removal of every trace of dust particles, need not concern us here.

It may be added that in the choice of solvents (usually buffers or other dilute salt solutions), in SAXS one is limited to fairly low salt concentrations. Since the scattering intensity is a function of electron density, the solvent scattering at high salt concentrations could easily mask the scattering of the sample. Furthermore, since X-ray scattering is a function of electron concentration, light ions are preferable to heavy ones; for example, fluoride should be used preferably to chloride.

b. Protein Concentration and Partial Specific Volume Determinations. Protein concentrations must be known with high precision, since accurate extrapolation to zero concentration is required, and concentration enters into the expression for the measurement of the molecular weight (see eq. 16), even at extrapolation to zero concentration. As in other protein work, careful ultraviolet absorbance measurements (See chapter of this volume) are the method of choice, provided the absorptivity at some given wavelength is known. Otherwise, dry weight measurements might be necessary.

The partial specific volume must also be known precisely, since it appears as the square in the molecular weight equation (eq. 18). At present, instrumentation is available to carry out such measurements to a precision of better than $\pm 0.2\%$ (See chapter of this volume and ref. 119).

c. Cell Thickness Measurement. Since the cell thickness determines the number of scatterers within the irradiated volume seen by the detector, it needs to be accurately known to permit expressing scattered intensities in terms of the scattering of a single electron; and, indeed, the cell thickness appears in the expression for the normalized intensities (see Sect. IV.A). Inasmuch as this thickness measurement is related to the construction of the cell, we shall digress briefly to describe the kinds of cell or sample container used in work with dilute solutions.

A cell must satisfy certain requirements with respect to optical path length, volume and windows. For an optimal signal-to-noise ratio, the path length should be so chosen as to result in a maximum ratio of scattering relative to absorption. This is a criterion generally taken into consideration in diffraction work.^{119a} For dilute protein solutions, the optimum path length works out to about 1 mm. The sample volume must be balanced between the geometric requirements of the X-ray beam (e.g., the infinite slit-height assumption) and the need to use the minimum amount of sample, biological material frequently being in scarce supply. The window material must be radiation stable and transparent, should not contribute disturbing scattering of its own, and should have sufficient rigidity to maintain a given geometric shape.

These requirements can be met by quartz capillaries, as used in diffraction work, and by assembled cells with flat win-

dows, which may be either demountable or cemented to an appropriate spacer and frame. The preferred window material is mica; mylar film has also been used but lacks the rigidity necessary to maintain a nearly flat configuration. Because round capillaries present problems in establishing the precise path length and irradiated volume, we have adopted the use of flat windows in a demountable cell of about 0.35 ml volume. The frame elements, windows and 1-mm spacer (preferably of Teflon) may be clamped together by machine screws. For uniformity in tightening, to assure leak tightness without causing undue distortion of the windows, we have adopted a screw-ring assembly similar to that of standard infrared absorption cells. Suitable changes in dimensions take into account the optical requirements of the thickness-measuring device to be described below, and the fact that the thick, rigid windows used in infrared work are here replaced by exceedingly fragile sheets of mica (ca. 0.0175 mm thick).

If, in addition to the concentration, the X-ray absorption coefficient of the solution is known from previous experiments, the sample thickness may be calculated by the use of Beer's law from intensity measurements taken on the same sample container filled with sample and solvent, in turn. However, an X-ray system cannot be relied upon to retain constant intensity between these two measurements without special precautions, nor is it always easy to obtain a reliable value for the absorption coefficient. A further complication stems from the fact that

the cell windows are somewhat elastic. This precludes an exactly reproducible path length for consecutive fillings with solutions of slightly different properties, such as density, viscosity and surface tension. Furthermore, the absorption is quite weak with cells used for scattering purposes, the path length being chosen in the first place to minimize the absorption vis-a-vis the scattering.

This may be done with an instrument of a type first used in Luzzati's laboratory which comprises two opposed microscopes with fine-focusing adjustments between which the filled sample cell is placed. The microscope optics are chosen to give a very shallow depth of field (below 10 μm), so that the position of the microscope tube, as measured by a suitable indicator, is a precise indication of its focal plane at any particular setting. One microscope remains fixed and serves to define a reference plane in space. One face of one window of the sample cell is brought into coincidence with this plane by means of an adjustable sample cell holder. The other microscope which had been previously zeroed by focusing on this same plane is then adjusted to focus on the appropriate face of the second cell window. The difference between the two positions of this microscope gives the sample thickness, after refractive index corrections for solution and window material.

4. Data Gathering

a. Primary Beam Intensities. If the stability of the X-ray source as well as that of the slit and detection systems could

be absolutely relied on, there would be a need to take only a single measurement of the primary beam intensity; this single value could then be applied to the difference between the observed values of solution and solvent scattering. As a matter of fact, however, even the best of systems must be expected to undergo some fluctuations (See Sect. III.A). That is why the defining equation for excess normalized scattering (eq. 32, below) shows the normalization involving the direct beam intensities performed separately for solution and for solvent, before one is subtracted from the other. This procedure, although it is not universally followed, is proper inasmuch as the scattered intensities for solution and solvent may be determined during widely separated time periods, when the beam intensity cannot be assumed to have been identical.¹²⁰

Ideally, the beam intensity should be recorded concurrently with that of the scattered radiation. In the absence of a monitor (See Sect. III.A) this is not possible. All that one can do is to sample the beam at times when it is practical. If step scanning is chosen, it is possible to intercalate beam intensity measurements between steps of the scattered intensity measurement. As it is not practical to do this too often, the adopted practice is to do it either at a few predetermined positions during the step scan, or else routinely at certain times of the day (e.g., at the beginning and end of the work day, and at noon). If continuous scans are chosen, it is not practical to interrupt a scan in progress, and one is limited to

making beam measurements before and after each scan. In our practice, which uses primarily continuous scanning, the integrated intensity of the direct beam is measured between $\pm 0.3^\circ$, at a scanning speed of $1/8^\circ$ per minute, using an appropriate filter to limit the count rate, as discussed in Section III.B.

b. Scattered Intensities. Disregarding possible hybrid systems, there are essentially two ways of scanning, referred to above: by steps, and continuously. Step scanning has certain advantages that have made it the method chosen in the majority of laboratories. With the prevalence of modern digital data processing equipment, it appears logical to acquire data in digital form, as is done in step scanning. Since this is a discrete sampling procedure, in which certain angular positions (usually, but not necessarily, equidistant) are preselected for counting for a fixed time or a fixed count, it would also seem to offer some saving in time.

However, some finite time during which no counting can take place is expended while the scanning arm slews from one position to the next. Furthermore, the number of points required for good definition of a curve is quite large (usually at least 100) and the counting time at each point needs to be quite long. For a relative error of 1%, a total count of 10,000 is required, giving a standard deviation of $10,000 \pm 100$, or 1%.⁴⁴ Along the tail of a scattering curve, which accounts for perhaps 75% of the entire scan, a count of, typically,

25 count/second may be expected, implying a counting time of $10,000/25 = 500$ seconds, or nearly 7 minutes, per point, exclusive of the time required for slewing. Along the steeper portions of the curve, counting times may be much shorter, but rapid changes in curvature would benefit from more closely spaced points. Flexible arrangements, which can take into account the requirements suggested by the shape of the curve and thus make more efficient use of time, have been used by Kratky and Kratky¹²¹ and others.¹²²

Regarding the digital character of the data, it should be borne in mind that, because of the random errors characteristic of scattering data, it is not possible to subject them to the required slit-smearing correction (Section IV) without prior smoothing; without smoothing, computational artifacts are prone to arise and the data become severely degraded. Despite continual attempts at developing computer-adaptable smoothing routines (e.g., Oelschlaeger,¹²³ Damaschun and Müller,¹²⁴), these efforts have not been successful enough to induce those in this field to abandon manual smoothing. This, of course, largely negates the potential advantages of automatic data processing.

Pending the development of more reliable smoothing methods, we have found it practical, for the most part, to retain the older practice of continuous scanning with strip chart recording, followed by manual smoothing of the graphic record, and finally

to digitization. The strip chart is required in any case, to check on the symmetry of the scan.

The readability of the record depends to a great extent on the choice of the time constant of the ratemeter whose output is recorded.¹²⁵ Too short a time constant causes a jittery and cluttered trace, obscuring the trends to be looked for; too long a time constant will distort the record. Choice of time constant is often regarded more as an art than a science, and certain rules of thumb are appealed to. It should be apparent, however, that scanning speed and receiving slit opening are the determinant variables, as discussed by Klug and Alexander¹²⁶. In consequence of the very weak observed intensities, scanning speeds in SAXS need to be much slower than is customary in diffraction work, speeds of 1/2 degree per hour being typical. At speeds as low as this (approximately 60-fold slower than would be typical in diffraction), much higher time constants are permissible. Whereas time constants between 0.5 and 16 seconds are customary in diffraction, and commercial diffraction apparatus rarely provides a time constant as high as 40, we have concluded that 200 seconds would not be excessive for SAXS. With appropriate instrument modification such values can be realized. We have found routinely that a time constant of 200 seconds is very satisfactory, since it produces a quiet, undistorted and interpretable record.

IV. Data Evaluation

It is evident from the discussion of the previous sections that the problem of data evaluation can be quite tedious. Due to the low count rates, it is necessary to use as many data points as possible. We have found it advantageous to utilize the continuous method of scanning rather than the discrete point method, which also allows a more efficient smoothing of the data. The only requirement for the continuous scanning method is the use of a sufficiently long time constant, i.e., of the order of 200 sec.

A. Ancillary Calculations

Since SAXS measures the scattering from the electrons in a particle (See Sect. II.A), it follows that all parameters must be expressed in the corresponding electron- \AA^3 and not gram-ml units. This unit transformation can be easily accomplished with the use of the following expressions.

The partial specific volume, \bar{V} , in units of ml/g, can be transformed to ψ , expressed in $\text{\AA}^3/\text{el}$, by

$$\psi = \bar{V} 10^{24}/q_p \quad (30)$$

Here, q_p is the number of electrons per gram of the protein. This can be readily calculated from the amino acid composition or an elemental analysis.

The protein concentration, c_e , in units of electrons protein per electron solvent, is given by

$$c_e = \frac{gq_p}{q_s - (q_s - q_p)g} \quad (31)$$

where q_s is the number of electrons per gram of solvent and g is the gram fraction of protein in units of gram protein per gram solvent.

Finally, the excess normalized scattering function, $j_n(s)$ is obtained from³

$$j_n(s) = \left[\frac{I(s)}{\lambda^2 t \rho_s (7.9 \times 10^{-26}) E_o \left(\frac{ds}{dt} \right) f} \right]_{\text{solution}}$$

(32)

$$\left[\frac{I(s)}{\lambda^2 t \rho_1 (7.9 \times 10^{-26}) E_o \left(\frac{ds}{dt} \right) f} \right]_{\text{solvent}}$$

where $I(s)$ is the scattered count rate at each value of s in counts/sec, which is averaged on both sides of the primary beam for each s , λ is the wavelength of the $\text{Cu } K_{\alpha 1}$ peak in \AA ,^{126a} t is the thickness of the filled cell in cm.; 7.9×10^{-26} is the value of the scattering of a single electron derived from Thompson's equation (See eq. 8); E_o is the total number of counts under the primary beam while scanning at a set rate of ds/dt ; f is the product of the filter factors used for attenuation purposes when measuring the energy of the primary beam, and ρ_s and ρ_1 are the densities of the solution and solvent, respectively, in $\text{el}/\text{\AA}^3$. These ^{can be} calculated from

$$\rho_i = \frac{d_i q_i}{10^{24}} \quad (33)$$

where q_i is the number of el/g and d_i is the density in the usual units of g/ml of material i , here solution and solvent.

When some seventy or more $j_n(s)$ values, ranging from approximately 0.25 to 5° , 2θ , are calculated, the data evaluation can begin. First a plot of $s^3 j_n(s)$ vs. s^3 is generated. A typical plot is shown in Fig. 12 for the scattering of lysozyme at various concentrations. The limiting slope of the curve at high s^3 gives δ^* while the intercept gives the A value (See eq. 20). The concentration dependences of these parameters are reflected in Fig. 12 by the change in the slope as well as the intercepts when going from 36 g/liter to 22 g/liter. The A parameter is used in the calculation of the surface, S , and the surface-to-volume ratio, S/V , of the scattering particle, while δ^* , a parameter which measures the contribution due to internal atom diffraction, must be subtracted from each $j_n(s)$ value (See eq. 9) to give the quantity $j_n^*(s)$ which is used for the rest of the calculations (eqs. 20, 21, 23).

B. Molecular Parameters

A Guinier plot is then constructed by plotting $\log_e j_n^*(s)$ vs. s^2 (Fig. 13). Here, it is important to recall that, by definition, this plot is linear at small values of s for a homogeneous substance. The appearance of non-linearity or multiple-linearity in this region implies that the system being measured is non-homogeneous. With a homogeneous system, the slope of the linear region generates the apparent radius of gyration, R_a , (eq. 11), while the intercept yields the $j_n(0)$

value. Fig. 13 shows the large concentration dependence of $j_n(0)$, which is reflected in the intercepts of the Guinier plots at concentrations from 45 to 21.6 g/liter, while the R_G values, proportional to the slope of a Guinier plot, are only mildly concentration dependent.

The non-linear portion of the curve gives rise to the residual function $\phi(s)$, (eq. 11) by subtracting the calculated Guinier function from each $j_n^*(s)$ value and fitting these results to a polynomial in s^2 , such that $\phi(s)$ is now defined as

$$\phi(s) = \sum_{i=0}^N a_i s^{2i} \quad (34)$$

The integral

$$Q = \int_0^{\infty} s j_n^*(s) ds \quad (35)$$

which has been termed the invariant, Q , by Porod¹²⁷ must now be evaluated before proceeding to the final calculations.

This is accomplished by substituting eq. 34 into eq. 11, which yields

$$j_n^*(s) = j_n^*(0) \exp \left[-4/3\pi^2 R_a^2 s^2 \right] + \sum_{i=0}^N a_i s^{2i} \quad (36)$$

Then, integrating according to eq. 35, the first term analyti-

cally and the second term from zero to a predetermined high angle, s_L , we find that

$$Q = \sqrt{3/\pi} j_n^*(0)/4R_a + \sum_{i=0}^N \frac{a_i}{2} s_L^{2(i+1)} \quad (37)$$

Here it is important to discuss the problems associated with the numerical analysis of the residual function and the invariant. In the first place, care must be taken when fitting the residual function to a polynomial. Only the best polynomial least-squares routine should be employed, since the data in this region are very imprecise. Secondly, the roots of the polynomial must be calculated in order to obtain a good value for s_L . It is possible to pick an erroneous value for which the residual function would already be negative. This would result in a value for the invariant which is much too small and which would lead to too large values of the hydrated volume, the surface-to-volume ratio and the degree of internal hydration and to a too small value of the electron density difference.

Using the same type of argument as was used in the calculation of the invariant, it is possible to derive from equations 12 and 36 the following expression for the deconvoluted scattering function,³

$$i_n(s) = 2 \sqrt{\pi/3} j_n^*(0) R_a \exp \left[-\frac{4}{3} \pi^2 R_a^2 s^2 \right] - \frac{1}{\pi} \sum_{i=0}^N 2ia_i \int_0^\infty (s^2 + l^2)^{-(i-1)} dl \quad (38)$$

The integral in the second term can be evaluated analytically by using a simple recursion formula (derived from integration-by-parts) which can be found in any mathematical table of integrals. However, since the numerical calculation of this term is rather lengthy, it would necessitate the use of a computer program. These desmeared scattering values are then used in a second Guinier plot for calculating the true radius of gyration, R_G , from the slope and $i_n(0)$ from the intercept.

In his original work, due to the lack of computer facilities, Luzzati¹²⁸ derived the expressions for $i_n(0)$ and R_G using a Maclaurin expansion of eq. 11.

They are

$$i_n(0) = 2 \sqrt{\pi/3} j_n^*(0) R_a - \frac{1}{\pi} \int_0^{\infty} s^{-2} \phi(s) ds \quad (39)$$

and

$$R_G = \frac{R_a^2 + \frac{9\sqrt{3}\pi}{16\pi^4} \frac{1}{j_n^*(0)R_a} \int_0^{\infty} s^{-4} \phi(s) ds}{1 - \frac{\sqrt{3}\pi}{2\pi^2} \frac{1}{j_n^*(0)R_a} \int_0^{\infty} s^{-2} \phi(s) ds} \quad (40)$$

By making use of the fact that the $\lim_{s \rightarrow \infty} s^3 j_n^*(s) = A$ (a constant), the integrals in eqs. 39 and 40 were approximated^{41, 42} by

$$\int_0^{\infty} s^{-2} \phi(s) ds \approx \sum_0^a s^{-2} \phi(s) \Delta s + \lim_{s \rightarrow \infty} s^3 j_n^*(s) \int_a^{\infty} \frac{ds}{s^5} \quad (41)$$

and

$$\int_0^{\infty} s^{-4} \phi(s) ds = \sum_0^a \frac{\phi(s)}{s^4} \Delta s + \lim_{s \rightarrow \infty} s^3 j_n^*(s) \int_a^{\infty} \frac{ds}{s^7} \quad (42)$$

where a is the value of s at which the scattering function $j_n^*(s)$ reaches, for all practical purpose, a constant limit. At very low values of s , $\phi(s)/s^2$ is obtained by interpolation between the measurable range of s and $s = 0$, since $\lim_{s \rightarrow 0} \phi(s)/s^2 = 0$. The function $\phi(s)/s^4$ attains a constant value at low s , and thus can be calculated between $s = 0$ and $s = a$.

It is interesting to note that the contribution of the integrals in eq. 39 and 40 is usually of the order of 1 to 3% for normal globular protein. This contribution increases, however, as the concentration of the protein solution increases, or as the molecules become larger and more asymmetric. Although the Luzzati expressions can be calculated on a desk calculator, it is preferable to use eq. 38 when a computer is available, since eqs. 39 and 40 were derived from an expansion in which all but the first two terms were dropped. It is quite possible that with larger, less globular proteins large errors will develop in eqs. 39-42; these might easily escape the cognizance of the investigator.

From the calculated values of $i_n(0)$, Q , and A , the rest of the structural parameters, namely, the molecular weight, M , the hydrated volume, V , the surface-to-volume ratio, S/V , the

electron density difference, and the degree of internal hydration, H , can be calculated by direct use of eqs. 18-25 at each protein concentration. Each parameter in turn, is extrapolated to zero protein concentration in order to cancel virial effects (See equations 16-19).

C. Typical Examples

Typical examples of results obtained using this type of analysis are given in Table I for ribonuclease, lysozyme and α -lactalbumin. The values of the various molecular parameters extrapolated to zero protein concentration show the close overall structural similarity between lysozyme and α -lactalbumin^{6,129} which is in essential agreement with the expectations raised by Browne et al,¹³⁰ who have postulated that the secondary and tertiary structures of these two proteins should be similar on the basis of their homologous amino acid sequences.¹³¹ The ribonuclease data for R_G , M , V , S/V and H , on the other hand, show the sensitivity of the small-angle X-ray scattering technique for distinguishing between globular proteins of the same general size but different conformations. The R_G values for the three proteins are almost the same, but the S/V and V parameters are significantly different. Thus, it can be concluded that lysozyme and α -lactalbumin are very similar proteins in their overall structures, while ribonuclease is different from both of them. Furthermore, the crystallographic radii of gyration have been calculated for ribonuclease by Kartha as 13.5 \AA ¹³² and for

lysozyme by Blake et al. as 13.8 \AA .¹³³ The solution values measured by SAXS are slightly higher. This could well be the result of the fact that SAXS gives the geometric parameters of the hydrated protein in solution, in which the surface side chains have much more freedom of motion¹³⁴ than in the crystalline state.

Another parameter which is useful in correlating SAXS data with other solution or crystallographic data is the axial ratio of an equivalent ellipsoid of revolution, a/b , where a is the major axis and b is the minor axis. This parameter can be calculated²⁴ from the products $(3V/4\pi R_G^3)$ and $R_G(S/V)$, respectively. A working graph, derived by Witz et al.²⁴, relating these quantities to the axial ratio is shown in Fig. 14. One ^{merely} / calculates the values for $(3V/4\pi R_G^3)$ and $(R_G(S/V))$ from small-angle X-ray scattering data extrapolated to zero protein concentration, and reads from the curves the corresponding values of the axial ratio, a/b , for a prolate and an oblate ellipsoid of revolution. Such a calculation was performed ^{for} / ribonuclease, lysozyme and α -lactalbumin and the results, assuming prolate ellipsoids, are shown in Table I.

It is interesting to note that the value for lysozyme calculated from $(3V/4\pi R_G^3)$ was found to be 1.42, whereas the crystallographic value reported by Blake et al. was 1.5.¹³³ This agreement is quite good. The value ^{for} / α -lactalbumin is 1.43, which again shows the close structural similarities between the two proteins. Ribonuclease, on the other hand, has

an axial ratio of 1.8 which is much higher than the other two proteins. This, however, is consistent with the crystallographic result which show a greater degree of asymmetry and consequently a larger axial ratio. It is striking to note that the axial ratios calculated from ($R_G(S/V)$) are all considerably larger for all three enzymes. This apparent anomaly is due to the fact that proteins are not solid geometric entities but do indeed consist of surfaces with many holes and clefts. Thus, for a given volume, the surface is considerably larger than what would be predicted for a corresponding ellipsoid of revolution. In this way it can be seen that SAXS is very sensitive to the surface topology of the molecules. This is brought out even more strikingly by the fact that the difference between the axial ratios calculated from the volume and the surface, is larger for ribonuclease, than for lysozyme and α -lactalbumin. This is a direct result of the fact that the ellipsoidal model is even more incorrect for ribonuclease than for the other two proteins, since in ribonuclease a single polypeptide chain does indeed protrude somewhat from the main body of the molecule.

D. Precautions

When the calculations which lead to the molecular parameters are carried out with a computer, great care must be taken in programming. Since the residual function is not theoretically defined in an analytic fashion and since the Guinier region varies in s position and magnitude with the type and concentration of

material to be investigated, a program must be written with a large amount of operator decision-making. A self-contained program could lead to errors in the values of various s limits arising from the small scattering values at high angles and low concentrations of protein.

It is also necessary to consider in detail the problem of poly-dispersity which up to now has been only mentioned. Since in a non-homogeneous system, the Guinier plot shows a double linear or non-linear character one attempts to fit the data to a double gaussian function,²⁴ assuming a two component system,

$$j_n^*(s) = A \exp\left[-\frac{4}{3}\pi^2 \alpha^2 s^2\right] + B \exp\left[-\frac{4}{3}\pi^2 \beta^2 s^2\right] + \phi(s) \quad (43)$$

where A , B , α and β are adjustable parameters which are related to $j_n(0)$ and the R_G values of the two components and $\phi(s)$ is the normal residual function. It has been shown²⁴ that $i_n(0)$ and R_G values can then be obtained from

$$i_n(0) = 2\sqrt{\pi/3} (A\alpha + B\beta) - \frac{1}{\pi} \int_0^\infty s^{-2} \phi(s) ds \quad (44)$$

and

$$R_G = \left[\frac{3}{4\pi^2} \left[\frac{8\pi^2}{3} \sqrt{\pi/3} (A\alpha^3 + B\beta^3) + \frac{3}{2\pi} \int_0^\infty s^{-4} \phi(s) ds \right] \left[i_n(0) \right]^{-1} \right]^{1/2} \quad (45)$$

These parameters are weight average values and must be used in conjunction with the protein concentration in order to find the intrinsic values of the two species. These are obtained from

$$X^2 = \frac{C_1 X_1^2 + C_2 X_2^2}{C_t} \quad (46)$$

$$C_t = C_1 + C_2$$

where X is the structural parameter (G_g , $i_n(o)$, etc) at C_t , the total concentration, X_1 and X_2 are the structural parameters of the individual species, and C_1 and C_2 are their mass concentrations. Since these equations are not analytic in their solutions for X_1 and X_2 , it becomes necessary to use a curve fitting routine or a series of tables in X_1 and X_2 , C_1 and C_2 which are calculated at each X and C_t . This, however, is extremely cumbersome and not very precise. Therefore, a large number of experiments at various concentrations must be performed when dealing with a polydisperse system. In such systems, it is very advantageous to employ other methods, such as sedimentation velocity or sedimentation equilibrium, to aid in finding the concentration distribution, i.e., C_1 and C_2 values at every C_t .

E. High Angle Region

The final discussion deals with the calculations at high protein concentrations (> 100 g/l) for the particle shape, which is reflected in the positions and magnitudes of maxima and minima that appear at high angles ($2\theta > 4^\circ$).¹ Two alternative methods for handling these calculations are in use currently. These will

be described in turn, allowing the reader to choose his preference.

The first method has been used primarily by the Kratky school.¹⁰⁵ In this method the experimental $j_n(s)$ values are convoluted (according to eq. 12) to give $i_n(s)$ (which is normalized to an intercept of unity) at each angle and compared with theoretical curves calculated for various models.¹³⁶⁻¹³⁹ Such a comparison is shown in Fig. 15, in which the normalized $i_n(s)$ values (expressed by the symbol ϕ) are plotted as a double logarithmic plot as a function of (sR_G) for experimental data obtained on yeast glyceraldehyde-3-phosphate dehydrogenase and compared with theoretical curves for various models. It is interesting to note that only a small maximum and minimum appear on the experimental curve. This is due to the low scattering intensities at high angles. The deconvolution integral (see eq. 12), first derivativizes then integrates a function, tending in the process to smear details of a curve, especially when the precision of the data is not maximal.

In the second method, proposed by Luzzati, the theoretical curves calculated for point source optics are transformed to slit optics.⁴¹ This approach makes it possible to compare the experimental scattering points, $j_n^*(s)$, directly with the theoretical curves for various models. The only transformation necessary in $j_n^*(s)$ is to normalize the function so that $i_n(0) = 1$. This is accomplished by

$$j(s) = \frac{j_n^*(s)}{c_e m(1-\rho_1 \psi)^2} \quad (47)$$

The quantity $j(s)$ is then plotted as function of (sR_G) on a double logarithmic plot and compared with the convoluted, or smeared, theoretical curves for various geometric models. Some of the convoluted scattering curves may be constructed from available tables;¹⁴⁰ others may be calculated by convoluting the $i_n(s)$ geometric model functions¹³⁶⁻¹³⁹ with the use of eq. 12. An example is shown in Fig. 16 for β -lactoglobulin at pH = 5.7 in 0.1 M acetate buffer.⁴¹ Here, the experimental $j(s)$ data are compared with various convoluted curves, namely those for the sphere, the two sphere and the parallelepiped models. The experimental curve shows large amplitudes of the maximum and the minimum, which have not been diminished by convolution of the data. It is obvious, however, that none of the geometric models fit the experimental scattering curve. This is in great part due to the nature of protein structure. Proteins, in general, are not smooth geometric bodies with uniform internal structures. Therefore, an exact fit of the experimental points to a geometric model should not be expected. Differences should indeed occur between these normalized theoretical and experimental curves and information on the overall gross structure, e.g. whether the protein structure lies between a single sphere and a two sphere model, should be ex-

pected.

Using the shape factor parameters and high angle data, together with calculated axial ratios at various conditions, such as pH, temperature, solvent composition, etc., an extremely large amount of information may be obtained on protein tertiary and quaternary structural changes and related to biological function.

V. Conclusion

In conclusion, it seems desirable to give some comparisons of the values of parameters measured with those obtained by other techniques. This can be readily done for the molecular weight and the radius of gyration. In Table II such a comparison is provided of the molecular weights and the Stokes radii calculated for equivalent spheres for several proteins. It is evident that good agreement of the molecular weight and radius of gyration can, in general, be obtained with other physical and chemical methods. This result gives confidence as well in the validity of the other molecular parameters which are measured, namely the hydrated volume, the surface to volume ratio and the degree of hydration, since these are derived from the same raw data.

References

1. A. Guinier and J. Fournet, "Small-Angle Scattering of X-rays." Wiley, New York, 1955.
2. W.W. Beeman, P. Kaesberg, J.S. Anderegg, and M.B. Webb, in "Handbuch der Physik" (S. Flügge, ed.), p. 321. Springer, Berlin, 1957.
3. V. Luzzati, Acta Crystallogr. 13, 939 (1960).
4. S.N. Timasheff, in "Electromagnetic Scattering" (M. Kerker, ed.), p. 337. Pergamon, New York, 1963.
5. S.N. Timasheff, J. Chem. Educ. 41, 314 (1964).
6. H. Pessen, T.F. Kumosinski, and S.N. Timasheff, J. Agr. Food Chem. 19, 698 (1971).
7. G. Fournet, Acta Crystallogr. 4, 293 (1951).
8. G. Fournet, Bull. Soc. Fr. Mineral. Cristallogr. 74, 37 (1951).
9. J.G. Kirkwood and J. Mazur, J. Polymer Sci. 9, 519 (1952).
10. P. Saludjian and V. Luzzati, in "Poly- α -amino acids" (G.D. Fasman, ed.), p. 157. Dekker, New York, 1967.

11. V. Luzzati, J. Witz, and R. Baro, J. Phys. (Paris), Suppl. 24, 141A (1963).
12. O. Kratky and H. Leopold, Makromol. Chem. 75, 69 (1964).
- 12a. Another distinct phenomenon is "inelastic" or "modified scattering", also termed "incoherent" because of its lack of definite phase relationships and "Compton scattering". It becomes more pronounced the higher the energy of the radiation (e.g. gamma rays), but is negligible at small angles. SAXS is concerned solely with elastic scattering.
13. W.H. Zachariasen, "Theory of X-ray Diffraction in Crystals." Wiley, New York, 1945.
14. This is the source of the loss of phase angle information in X-ray diffraction.
15. The angle 2θ is equal to twice the reflection, or Bragg, angle which is familiar with X-ray diffraction.
16. Comparison of equations 5 and 7 reveals a notable difference between the wavelength dependences of light scattering and small-angle X-ray scattering. The Rayleigh equation

(eq. 5) contains the well-known inverse fourth power of wavelength dependence of light scattering. In the Thompson equation (eq. 7) no such relationship appears, i.e., X-ray scattering intensities are not wavelength dependent. This difference derives from the circumstance that in the Rayleigh equation the polarizability, which appears squared in the numerator, is not a simple function of wavelength; for X-rays, however, the polarizability is proportional to the square of the wavelength (See eq. 6), allowing all the wavelength terms to cancel from the equation.

17. This is also the origin of the term "electron density map" used in X-ray diffraction.
18. P. Debye, Ann. Phys. (Leipzig), 46, 809 (1915).
19. A. Guinier, Ann. Phys. (Paris), 12, 161 (1939).
20. The notation adopted in this presentation is that due to Luzzati³. A variety of other notations have been used in the literature. These, in general, refer to intensity normalized in different ways and to different ways of expressing

the angular function. The most common alternate notations either use the Bragg angle θ as such, or the symbol h , defined as $h = \frac{4\pi\sin\theta}{\lambda}$.

21. W. Kauzmann, "Quantum Chemistry." Academic Press, New York, 1957.
22. C. Tanford, "Physical Chemistry of Macromolecules." Wiley, New York, 1961.
23. This equation is analogous to the light scattering equation, with electron density increment replacing refractive index increment.
24. V. Luzzati, J. Witz, and A. Nicolaieff, J. Mol. Biol. 3, 367 (1961).
25. G. Porod, Kolloid - Z. 124, 83 (1951).
26. J. L. Soulé, J. Phys. Radium, Phys. Appl. Suppl. 18, 90A (1957).
27. G. Scatchard, J. Amer. Chem. Soc. 68, 2315 (1946).
28. W.H. Stockmayer, J. Chem. Phys. 18, 58 (1950).

29. S.N. Timasheff and R. Townend, in "Physical Principles and Techniques of Protein Chemistry" (S.J. Leach, ed.), Part B, p. 147. Academic Press, New York, 1970.
30. E.P. Geiduschek and A. Holtzer, Advan. Biol. Med. Phys. 6, 431 (1958).
31. H. Sund, I. Pilz, and M. Herbst, Eur. J. Biochem. 7, 517 (1969).
32. V. Luzzati, A. Nicolaieff, and F. Masson, J. Mol. Biol. 3, 185 (1961).
33. V. Luzzati and H. Benoit, Acta Crystallogr. 14, 297 (1961).
34. C. Sadron and J. Pouyet, Proc. 4th Intern. Congr. Biochem., Vienna, Vol. 9, p. 52. Pergamon Press, Oxford, 1958.
35. M.J. Kronman, S.N. Timasheff, J.S. Colter, and R.A. Brown, Biochim. Biophys. Acta 40, 410 (1960).
36. S.N. Timasheff, J. Witz, and V. Luzzati, Biophys. J. 1, 526 (1961).
37. S.N. Timasheff, Biochim. Biophys. Acta 88, 630 (1964).
38. D.E. Roark and D.A. Yphantis, Ann. N.Y. Acad. Sci. 164, 245, (1969).

39. S.N. Timasheff and R. Townend, J. Amer. Chem. Soc. 83, 464 (1961).
40. T.F. Kumosinski and S.N. Timasheff, J. Amer. Chem. Soc. 88, 5635 (1966).
41. J. Witz, S.N. Timasheff, and V. Luzzati, J. Amer. Chem. Soc. 86, 168 (1964).
42. M. Bier, in "Methods in Enzymology" (S.P. Colowick and N.O. Kaplan, eds.), Vol. 4, p. 165. Academic Press, New York, 1957.
43. K.A. Stacey, "Light Scattering in Physical Chemistry," Chap. 3. Academic Press, New York, 1956.
44. H.P. Klug and L.E. Alexander, "X-Ray Diffraction Procedures," p. 270. Wiley, New York, 1954.
45. O. Kratky, in "Small-Angle X-Ray Scattering" (H. Brumberger, ed.), p. 64. Gordon and Breach, New York, 1967.
46. T.W. Baker, J.D. George, B.A. Bellamy, and R. Causey, in "Advances in X-Ray Analysis" (J.B. Newkirk, G.R. Mallett, and H.G. Pfeiffer, eds.), Vol. 11, p. 361. Plenum Press, New York, 1968.

47. W.W. Beeman, in "Small-Angle X-Ray Scattering" (H. Brumberger, ed.), p. 197. Gordon and Breach, New York, 1967.
48. O. Kratky, H. Leopold, and H.-P. Seidler, Z. Angew Phys. 31, 49 (1971).
49. C.R. Peters and M.E. Milberg, Rev. Sci. Instrum. 37, 1186 (1966).
50. M. Berman and S. Ergun, Rev. Sci. Instrum. 40, 1144 (1969).
51. See reference 1, p. 85.
52. See reference 144, p. 81.
53. D.R. Chipman, in "Methods of Obtaining Monochromatic X-Rays and Neutrons" (F. Herbstein, ed.), pp. 55-58. Union Crystallogr., Utrecht, Netherlands, 1967.
54. J. Witz, Acta Crystallogr. A25, 30 (1969).
55. H.H. Johann, Z. Phys. 69, 185 (1931).
56. T. Johansson, Naturwissenschaften 20, 758 (1932).
57. T. Johansson, Z. Phys. 82, 507 (1933).
58. A. Guinier, C. R. H. Acad. Sci. 223, 31 (1946).
59. V. Gerold, Acta Crystallogr. 10, 287 (1957).

60. W. Ruland, Acta Crystallogr. 17, 138 (1964).
61. J. Mazur and A.M. Wims, J. Res. Nat. Bur. Stand. 70A, 467 (1966).
62. P. W. Schmidt, Acta Crystallogr. 8, 772 (1955).
63. S. Heine, Acta Phys. Austr. 16, 144 (1963).
64. B. Chu and D.M. Tan Creti, Acta Crystallogr. 18, 1083 (1965).
65. J.A. Lake, Acta Crystallogr. 23, 191 (1967).
66. O. Kratky, G. Porod, and Z. Skala, Acta Phys. Austr. 13, 76 (1960).
67. D.P. Riley, in "X-Ray Diffraction by Polycrystalline Materials" (H.S. Peiser, H.P. Rooksby, and A.J.C. Wilson, eds.), p. 439. Inst. Phys., London, 1955.
68. V. Luzzati, Acta Crystallogr. 13, 939 (1960).
69. O. Kratky and H. Wawra, Monatsh. Chem. 94, 981 (1963).
70. R.W. Hendricks, J. Appl. Crystallogr., in press.
71. H. Witte and E. Wölfel, Rev. Mod. Phys. 30, 51 (1958).
72. D.L. Weinberg, Rev. Sci. Instrum. 34, 691 (1963).
73. G. Damaschun and J. Müller, Z. Naturforsch. 20a, 1274 (1965).

74. H. Pessen, T.F. Kumosinski, S.N. Timasheff, R.R. Calhoun, Jr., and J.A. Connelly, in "Advances in X-Ray Analysis" (B.L. Henke, J.B. Newkirk, and G.R. Mallet, eds.), Vol. 13, pp. 622, 626. Plenum Press, New York, 1970.
75. B.W. Batterman, D.R. Chipman, and J.J. DeMarco, Phys. Rev. 122, 68 (1961).
76. O. Kratky, Z. Anal. Chem. 201, 161 (1964).
77. O. Kratky, I. Pilz, and P.J. Schmitz, J. Colloid Interface Sci. 21, 24 (1966).
78. I. Pilz and O. Kratky, J. Colloid Interface Sci. 24, 211 (1967).
79. I. Pilz, J. Colloid Interface Sci. 30, 140 (1969).
80. L. Katz, "Absolute Intensity Measurements of Small-Angle X-Ray Scattering." Ph.D. Thesis, University of Wisconsin, 1959.
81. L.B. Shaffer, "Absolute X-Ray Scattering Cross Sections of Liquids and Solutions." Ph.D. Thesis, University of Wisconsin, 1964.

82. L.B. Shaffer and W.W. Beeman, J. Appl. Crystallogr. 3, 379 (1970).
83. O. Kratky, G. Porod, and L. Kahovec, Z. Elektrochem. 55, 53 (1951).
84. P.H. Hermans, D. Heikens, and A. Weidinger, J. Polymer Sci. 35, 145 (1959).
85. I.S. Patel and P.W. Schmidt, J. Appl. Crystallogr. 4, 50 (1971).
86. O. Kratky and Z. Skala, Z. Electrochem. Ber. Bunsenges. Phys. Chem. 62, 73 (1958).
87. W. Parrish, E.A. Hamacher, and K. Lowitzsch, Philips Technical Review 16, 123 (1954).
- 87a. From this configuration, the occasional use of the alternative designation of "low-angle" scattering for SAXS is readily understood.
88. If the tube focus is rectangular, as is usually the case, one pair of opposing windows will present horizontal line sources; the other pair, because of foreshortening, will

present square or spot sources. While only the former are usable for scattering instruments requiring slit sources, the other two ports remain available for other apparatus.

89. O.E.A. Bolduan and R.S. Bear, J. Appl. Phys. 20, 983 (1949).
90. K.L. Yudowitch, J. Appl. Phys. 20, 1232 (1949).
91. See reference 1, pp. 86 ff.
92. R. Hosemann, Ergeb. Exakt. Naturwissenschaften 24, 142 (1951).
93. See reference 47, p. 198.
94. J.W. Anderegg, W.W. Beeman, S. Shulman, and P. Kaesberg, J. Amer. Chem. Soc. 77, 2927 (1955).
95. H.N. Ritland, P. Kaesberg, and W.W. Beeman, J. Chem. Phys. 18, 1237 (1950).
96. R.T. Brierre, "Small-Angle X-Ray Scattering Investigation of Proteins in Solution." Ph.D. Thesis, Duke University, 1965.
97. L. Kahovec and H.F. Ruck, Z. Elektrochem. 57, 859 (1953).
98. I. Fankuchen, Nature (London) 139, 193 (1937).
99. See reference 1, pp. 100 ff.

100. See reference 74, pp. 618-631.
101. A. Renouprez, H. Bottazzi, D. Weigel, and B. Imelik,
J. Chim. Phys. 62, 131 (1965).
102. S. Kavesh and J.M. Schultz, Rev. Sci. Instrum. 40, 98 (1969).
103. O. Kratky and W. Kreutz, Z. Electrochem. Ber. Bunsenges.
Phys. Chem. 64, 880 (1960).
104. I. Pilz, O. Kratky, F. von der Haar, and F. Cramer, Eur. J.
Biochem. 18, 436 (1971).
105. H. Durschschlag, G. Puchwein, O. Kratky, I. Schuster, and
K. Kirschner, Eur. J. Biochem. 19, 9 (1971).
106. S. Hagström and K. Siegbahn, J. Ultrastruct. Res. 3, 401
(1960).
107. B.L.Henke and J.W.M. DuMond, J. Appl. Phys. 26, 903 (1955).
108. L. Shenfil, W.E. Danielson, and J.W.M. DuMond, J. Appl.
Phys. 23, 854 (1952).
109. T.C. Furnas, Jr., Rev. Sci. Instrum. 28, 1042 (1957).
110. A. Franks. Brit. J. Appl. Phys. 9, 349 (1958).
111. A. Elliott, J. Sci. Instrum. 42, 312 (1965).

112. H. Brumberger and R. Deslattes, J. Res. Nat. Bur. Stand. 68C, 173 (1964).
113. U. Bonse and M. Hart, in "Small-Angle X-Ray Scattering" (H. Brumberger, ed.), pp. 121-130. Gordon and Breach, New York, 1967.
114. D.M. Koffman, in "Advances in X-Ray Analysis" (J.B. Newkirk, G.R. Mallett, and H.G. Pfeiffer, eds.), Vol. 11, pp. 332-338. Plenum Press, New York, 1968.
115. O. Kratky and H. Leopold, Makromol. Chem. 133, 181 (1970).
116. See reference 44, p. 281.
117. P.R. Chipman, Acta Crystallogr. A25, 209 (1969).
118. A. Guinier, "Theorie et Technique de la Radiocristallographie," p. 192. Dunod, Paris, 1964.
119. D.W. Kupke and J.W. Beams, in "Methods in Enzymology" (C.H.W. Hirs and S.N. Timasheff, eds.), Vol. 26, Chapt. 5. Academic Press, New York, 1972.
- 119a. See reference 44, p. 205.

120. This is the basis for the difference between our statement

(See Sect. I) that a number of parameters may be obtained

only from absolute measurements and occasional statements

in the literature which imply that, except for molecular

weight, other molecular parameters beyond radius of gyra-

tion are obtainable from relative measurements alone.

Correct as this may be in principle, it is not realistic

in view of what has been said above regarding the opera-

tional equation (32) and the possibility of long term shifts

in the intensity of the primary beam.

121. Ch. Kratky and O. Kratky, Z. Instrumentenkunde 72, 302 (1964).

122. H. Leopold, Z. Angew Phys. 25, 81 (1968).

123. H. Oelschlaeger, Acta Phys. Austr. 30, 323 (1969).

124. G. Damashun, J.J. Müller, and H.-V. Pürschel, Acta Crystallogr. A27, 11 (1971).

125. Similar remarks would apply to the gating times of an electronic counter used in conjunction with a digital-to-analog converter, optionally used in place of the more conventional ratemeter.

126. See reference 44, p. 310.

126a. The presence of λ^2 in the denominator of eq. 32 does not mean that the scattering intensity is a function of wavelength, seemingly contradicting eq. 7. In eq. 32, λ^2 appears trivially as a conversion factor between $(2\theta)^2$

and s². 126b

126b. See reference 1, p. 18.

127. G. Porod, Kolloid-Z. 124, 83 (1951); 125, 51 (1952).

128. V. Luzzati, Acta Crystallogr. 11, 843 (1958).

129. H. Pessen, T.F. Kumosinski, and S.N. Timasheff, Fed. Proc.

30, 1180 Abs. (1971).

130. W.J. Browne, A.C.T. North, D.C. Phillips, K. Brew, T.C.

Vanaman, and R.L. Hill, J. Mol. Biol. 42, 65 (1969).

131. K. Brew, T.C. Vanaman, and R.L. Hill, J. Biol. Chem. 242,

3747 (1967).

132. G. Kartha, J. Appl. Crystallogr. 4, 417 (1971).

133. C.C.F. Blake, D.F. Koenig, G.A. Mair, A.C.T. North, D.C.

Phillips, and V.R. Sarma, Nature (London) 206, 757 (1965).

134. K.V. Linderstrøm-Lang and J.A. Schellman, in "The Enzymes"

(P.D. Boyer, H. Lardy and K. Myrbäck, eds.), Chapt. 10.

Academic Press, New York, 1959.

135. G. Kartha, J. Bello, and D. Harker, Nature (London) 213,

862 (1967).

136. O. Kratky and G. Porod, Acta Phys. Austr. 2, 133 (1948).

137. G. Porod, Acta Phys. Austr. 2, 255 (1948).

138. P. Mittelbach and G. Porod, Acta Phys. Austr. 14, 185,

405 (1961); 15, 122 (1962).

139. P. Mittelbach, Acta Phys. Austr. 19, 53 (1964).

140. P.W. Schmidt, Acta Crystallogr. 8, 772 (1955).

141. V. Luzzati, J. Witz, and A. Nicolaieff, J. Mol. Biol. 3,

379 (1961).

142. W.R. Krigbaum and R.W. Godwin, Biochemistry 7, 3126 (1968).

Table I

	<u>STRUCTURAL PARAMETERS</u>		
	<u>RIBONUCLEASE</u>	<u>LYSOZYME</u>	<u>α-LACTALBUMIN</u>
$R_G, \text{ \AA}$	14.8	14.3	14.5
M	12,700	13,600	13,500
$V, \text{ \AA}^3$	22,000	24,200	25,100
$S/V, \text{ \AA}^{-1}$	0.29	0.25	0.24
$H, g_{H_2O}/g_{prot}$	0.46	0.33	0.37
A/B From $(\frac{3V}{4\pi R_G^3})^a)$	1.87	1.42	1.43
A/B From $(R_G \frac{S}{V})^a)$	3.70	2.92	2.82

a) Assuming a prolate ellipsoid of revolution

Table II

Comparison of SAXS Results With Those of Other Techniques

Protein	Molecular Weight		Stokes Radius (r)		
	Small-Angle X-Ray Scattering	Amino Acid Composition	Small-Angle X-Ray Scattering ^(a)	Sedimentation Velocity ^(b)	Titration ^(c)
Ribonuclease	12,700 ^(d)	13,800	19.1 ⁶	22.4	20.7
Lysozyme	13,600 ⁶	14,300	18.5 ⁶	18.8	17.9
α -Lactalbumin	13,500 ⁶	14,500	18.5 ⁶	18.8	--
Bovine Serum Albumin	81,200 ¹⁴¹	77,000 ^(e)	39.5 ¹⁴¹	38.3	38.2
β -Lactoglobulin Dimer	36,600 ⁴¹	36,300	27.7 ⁴¹	27.0	27.0
β -Lactoglobulin A Octamer	(144,000) ⁴¹	(145,200)	44.4 ⁴¹	43.3	43.8
α -Chymotrypsin	22,000 ¹⁴²	25,200	23.3 ¹⁴²	23.5	--

(a) Calculated from: $r = \left(\frac{5}{3}\right)^{1/2} R_G$

(b) Calculated from: $r = \frac{M(1 - \bar{v}_2\rho)}{6\pi\eta N_A s_{20,w}^o}$

(η : solution viscosity, $s_{20,w}^o$ = sedimentation coefficient), see²².

(c) Calculated from: $\frac{1}{r} = \frac{2DkTw}{e^2} + \frac{\kappa}{1+\kappa a}$

(D, dielectric constant; k, Boltzmann constant; T, absolute temperature; e, electronic charge = 4.8×10^{-10} e.s.u., w = electrostatic work function derived from the titration curve; X, Debye-Huckel screening parameter, a = center-to-center distance of closest approach between protein and small buffer ion), see²².

(d) Recalculated from ref. 6.

(e) The molecular weight of bovine serum albumin is 69,000; however, for the sake of comparison with the \bar{M}_w value obtained in small-angle X-ray scattering, the contribution from 5% dimer, normally present, has been taken into account.

Legends

Figure 1: Fundamentals of small-angle X-ray scattering.

A. Basic "scattering" event; B. Definition of terms.

Figure 2: Angular dependence of scattering. A. Internal interference; B. Scattering envelope; C. Schematic representation of typical recording of data.

Figure 3: Types of plots used in small-angle X-ray scattering. A. Guinier plot; B. Soule-Porod plot.

Figure 4: Comparison of resolutions obtained with light scattering and small-angle X-ray scattering.

Figure 5: Comparison of concentration ranges covered by sedimentation equilibrium, light scattering and small-angle X-ray scattering.

Figure 6: Johann bent-crystal monochromators: (a) symmetrical; (b) asymmetrical. S, source; F, focus; C, circumference of Rowland circle; R, radius of curvature of crystal. (From ref. 55.)

Figure 7: Schematic top view of X-ray tube and four-slit scattering geometry. (From ref. 47.)

Figure 8: Schematic diagram of system employing bent-crystal monochromator. C, crystal; F, film plane. (From ref. 99.)

Figure 9: Schematic top view of scattering apparatus with monochromator and four slits. X, X-ray source; MC, monochromator; S_1 , S_2 , beam-defining slits; SC, sample cell; S_3 , receiving slit; S_4 , anti-scatter slit; D,

detector. (From ref. 6.)

Figure 10: Kratky collimation system. D_1 , entrance block; D_2 , U-shaped block; D_3 , bridge block; S, entrance opening slit; E_1 , E_2 , E_3 , edges; H, principal section. (From ref.

Figure 11: Multiple reflection diffractometer according to Bonse-Hart. Each grooved crystal contains five Bragg reflections. (From ref. 113.)

Figure 12: Computer plots of $s^3 j_n(s)$ vs. s^3 for lysozyme at various protein concentrations. (From ref. 6.)

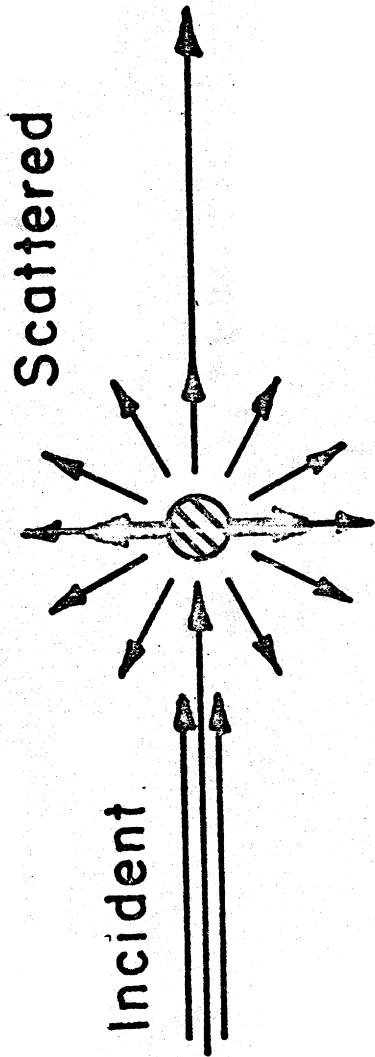
Figure 13: Guinier plots for lysozyme at several protein concentrations. (From ref. 6.)

Figure 14: Nomogram relating the geometric parameters of ellipsoids of revolution to the axial ratio, a/b . (From ref. 24.)

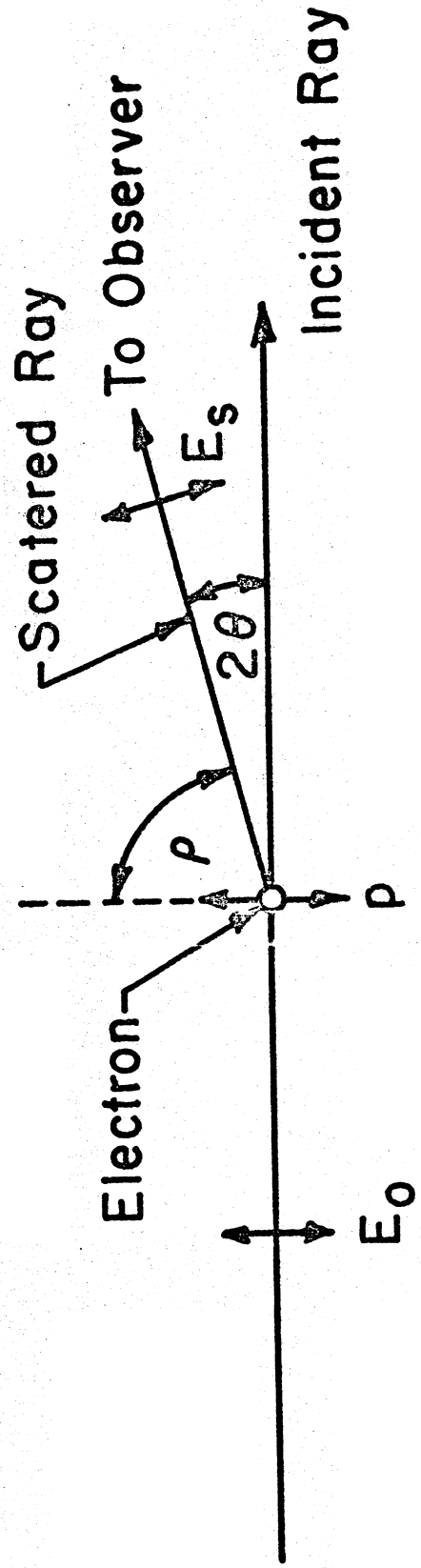
Figure 15: Log ϕ vs. log (sR) plot for comparison of the experimental scattering curve for the apo-enzyme of yeast glyceraldehyde-3-phosphate dehydrogenase in 50 mM sodium pyrophosphate, 5 mM Na EDTA and 0.2 mM dithiothreitol at pH 8.5 with theoretical scattering curves of model bodies built up from four rotation ellipsoids. T1, T2 tetrahedral configuration of the subunits; Q1, Q2, Q3, quadratic configuration of the subunits. (From ref. 105.)

Figure 16: Normalized scattering of β -lactoglobulin A and B in the higher angle range in 0.1 M sodium acetate at pH 5.7. The dashed line represents the experimental curve and the solid lines represent the convoluted theoretical curves calculated for various models. (From ref. 41.)

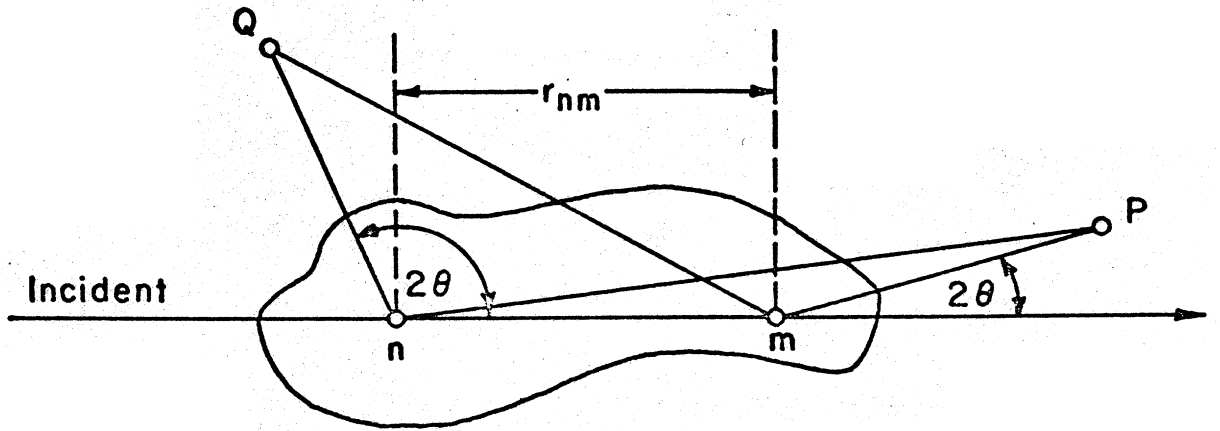
A



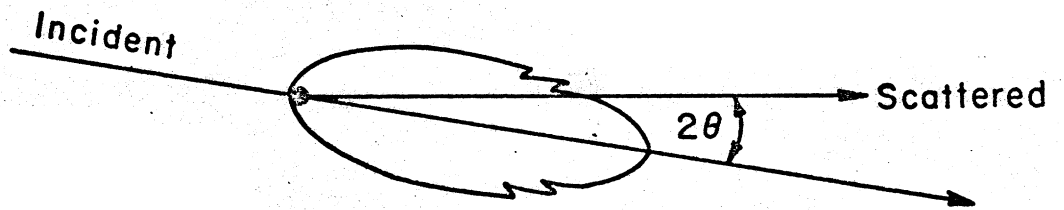
B



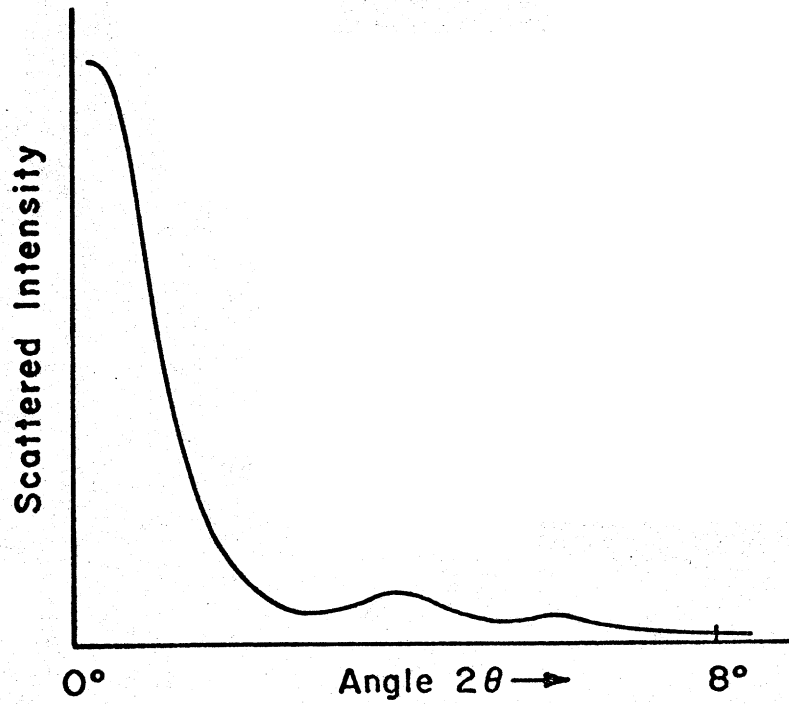
A



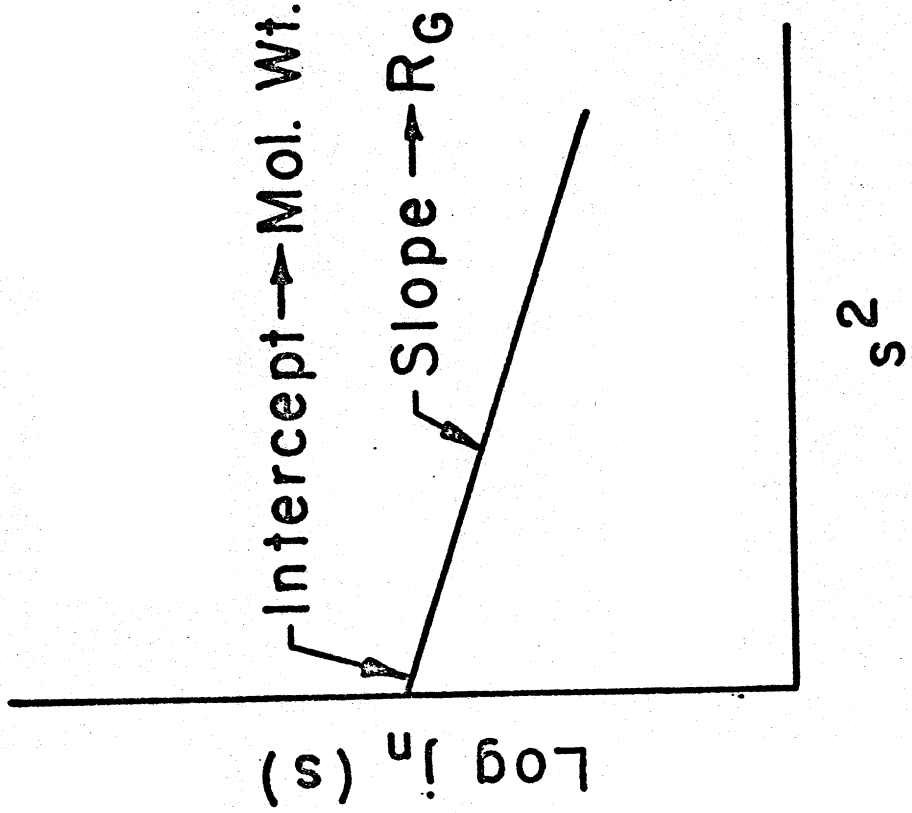
B



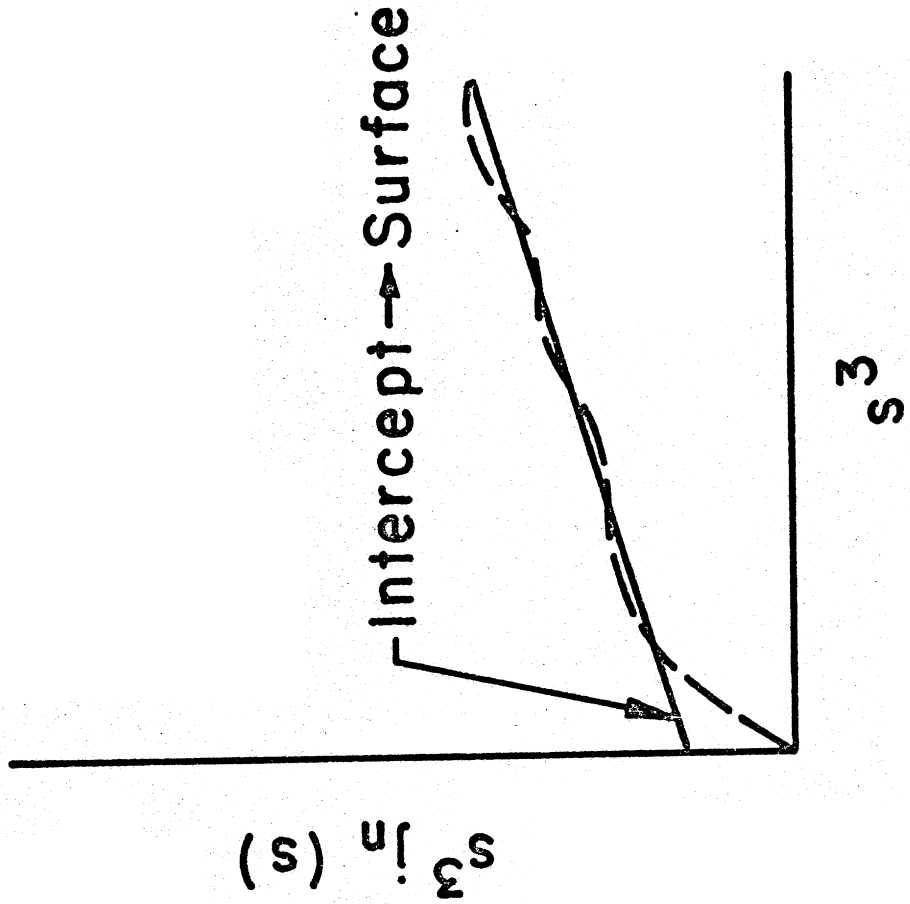
C



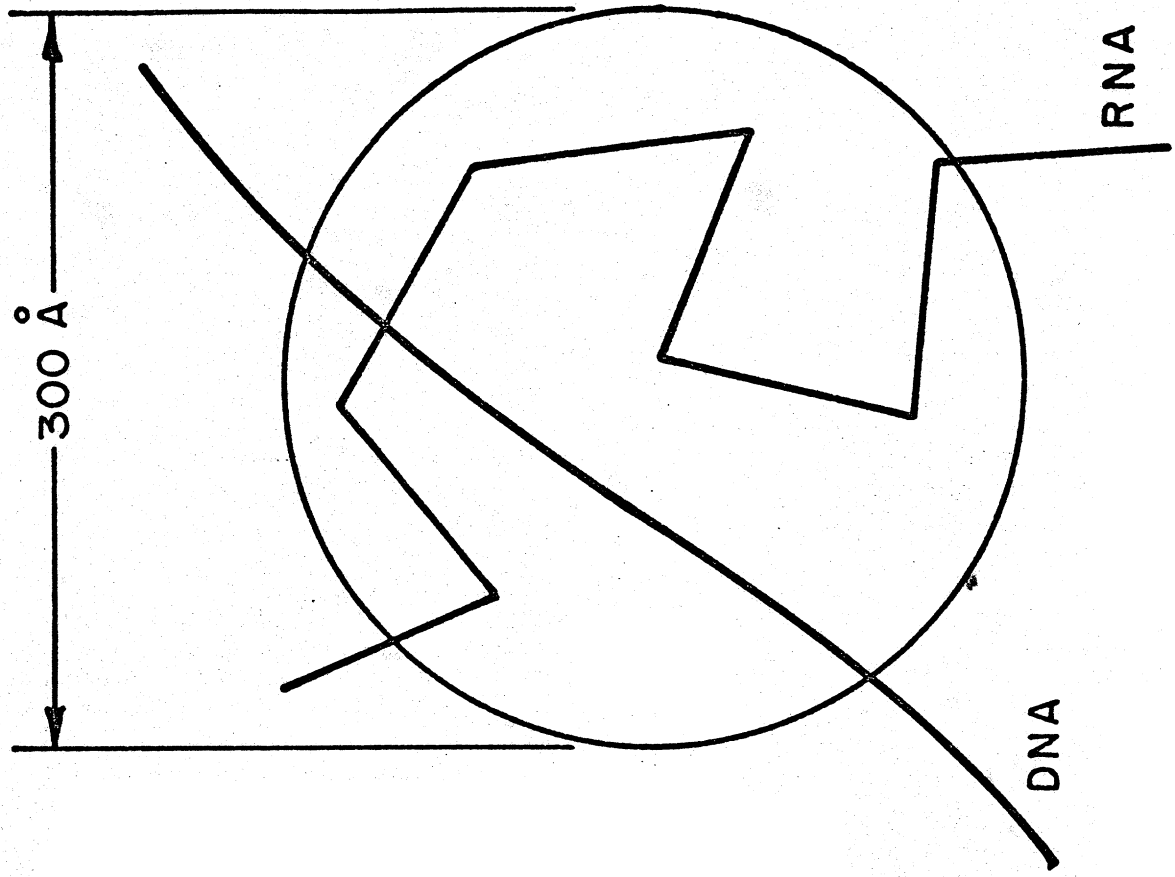
A



B



SMALL-ANGLE
X-RAY SCATTERING



LIGHT SCATTERING

